Avoiding Clinical Misinterpretation and Artifacts of Optical Coherence Tomography Analysis of the Optic Nerve, Retinal Nerve Fiber Layer, and Ganglion Cell Layer

John J. Chen, MD, PhD, Randy H. Kardon, MD, PhD

Background: Optical coherence tomography (OCT) has become an important tool for diagnosing optic nerve disease. The structural details and reproducibility of OCT continues to improve with further advances in technology. However, artifacts and misinterpretation of OCT can lead to clinical misdiagnosis of diseases if they go unrecognized.
Evidence Acquisition: A literature review using PubMed combined with clinical and research experience.
Results: We describe the most common artifacts and errors in interpretation seen on OCT in both optic nerve and ganglion cell analyses. We provide examples of the artifacts, discuss the causes, and provide methods of detecting them. In addition, we discuss a systematic approach to OCT analysis to facilitate the recognition of artifacts and to avoid clinical misinterpretation.
Conclusions: While OCT is invaluable in diagnosing optic nerve disease, we need to be cognizant of the artifacts that can occur with OCT. Failure to recognize some of these artifacts can lead to misdiagnoses and inappropriate investigations.

Optical coherence tomography (OCT) was first introduced in 1991 as a way of analyzing layers of the retina using interference patterns of reflected light (1). In 2002,

Department of Ophthalmology (JJC), Mayo Clinic, Rochester, Minnesota; Department of Ophthalmology and Visual Sciences (JJC, RHK), University of Iowa, Iowa City, Iowa; and Department of Veterans Affairs (RHK), Center for the Prevention and Treatment of Visual Loss, Iowa City, Iowa.

The authors report no conflicts of interest.

Address correspondence to Randy H. Kardon, MD, PhD, Department of Ophthalmology and Visual Sciences, University of Iowa Hospitals and Clinics, 200 Hawkins Drive PFP, Iowa City, IA 52242; E-mail: randy-kardon@uiowa.edu

OCT became much more commonplace with the introduction of Stratus OCT (Carl Zeiss Meditec, Dublin, CA), which utilized time-domain technology. An OCT machine is now in almost every ophthalmology clinic and has become a useful ancillary tool to provide in vivo structural information of the eye, which facilitates the ability to diagnose and monitor many retinal and optic nerve diseases, including glaucoma, optic neuritis, macular edema, and macular degeneration.

Spectral domain OCT has largely supplanted time-domain OCT because it allows for faster scans and higher resolution. Time-domain OCT obtained approximately 400 A-scans per second, while spectral domain OCT is able to obtain 20,000–40,000 A-scans per second, which provides an axial resolution on the order of 4–6 μm (2). Future OCT technology, such as swept source imaging, will invariably supplant spectral domain OCT and provide even better resolution, faster scanning, and repeatability.

While the initial OCT evaluation of the optic nerve was limited to measuring the retinal nerve fiber layer (RNFL), some OCT algorithms are now able to measure the disc area and rim area to help with the diagnosis of glaucoma (3). In addition, some OCT platforms are able to measure the macular ganglion cell layer-inner plexiform layer (GCL-IPL) in order to evaluate the cells that give rise to the optic nerve. Thinning of the macular GCL-IPL has been found to have a strong relationship with visual loss in optic nerve diseases such as glaucoma, optic neuritis, ischemic optic neuropathy, hereditary optic neuropathy, toxic optic neuropathy, optic nerve glioma, and idiopathic intracranial hypertension (4–12).

Despite improvements in OCT technology, the user must be able to accurately interpret the data and be aware of possible artifacts that can introduce a false-positive or negative diagnosis. For example, Kim et al (13) analyzed the RNFL of 149 eyes from 77 healthy adults with spectral domain OCT and found a false-positive rate of 26.2% (13). Another study by Asrani et al (14) found that there were spectral domain OCT imaging-related artifacts in 15.2%–36.1% of patients

being evaluated for glaucoma. Segmentation of the macula and measurements of the GCL-IPL complex is prone to error and misinterpretation, especially in eyes with pathology (e.g., age-related macular degeneration, optic disc edema). Even among healthy eyes, Kim et al (15) found that 40.4% had artifacts in the ganglion cell analysis. Therefore, over a quarter of patients will have artifacts of the RNFL and/or GCL analysis with spectral domain OCT. Being able to distinguish artifact from true disease becomes imperative in the care of the patient and can prevent further unnecessary, expensive investigations.

This is a review of the most common artifacts and misinterpretations that can occur in posterior segment OCT for optic nerve and ganglion cell layer analysis. We also discuss factors that influence repeatability of subsequent scans. Lastly, we provide a systematic approach to interpreting OCT analysis.

OPTIC DISC SCAN OPTICAL COHERENCE TOMOGRAPHY ANALYSIS

There can be artifacts in 1) measurement of total RNFL thickness, 2) interpretation of the spatial distribution of the RNFL bundles, and 3) interpretation of optic disc size and cupping. Factors that can confound the RNFL analysis includes wrongly entered age of the patient, poor signal strength, inaccurate segmentation of the retinal layers, long or short axial eye lengths, interindividual differences in the spatial distribution of nerve fiber bundles (developmental), cyclotorsion, peripapillary atrophy, ocular diseases that can cause an artifactual increase in RNFL thickness, and differences in the RNFL thickness among normal individuals. In addition, some of these factors will influence the measurement of the optic disc size, rim diameter, and cup. These are discussed individually.

Age of the Patient

The thickness measurements obtained from OCT machines are compared against age-matched controls in order to identify significant thinning or thickening. With aging, there is a natural attrition of the RNFL (16,17). One study demonstrated that the overall mean RNFL thickness on OCT decreases by 0.365 μm for every 1 year increase in age (18). Therefore, not accounting for age effects can significantly affect the estimate of disease progression (19). Entering the incorrect date of birth could cause abnormalities in the probability plots of the thickness measurements that could lead to erroneous interpretation.

Errors in Segmentation of the Retinal Nerve Fiber Layer: Media Opacity, Optic Nerve Edema, and Truncation of Image
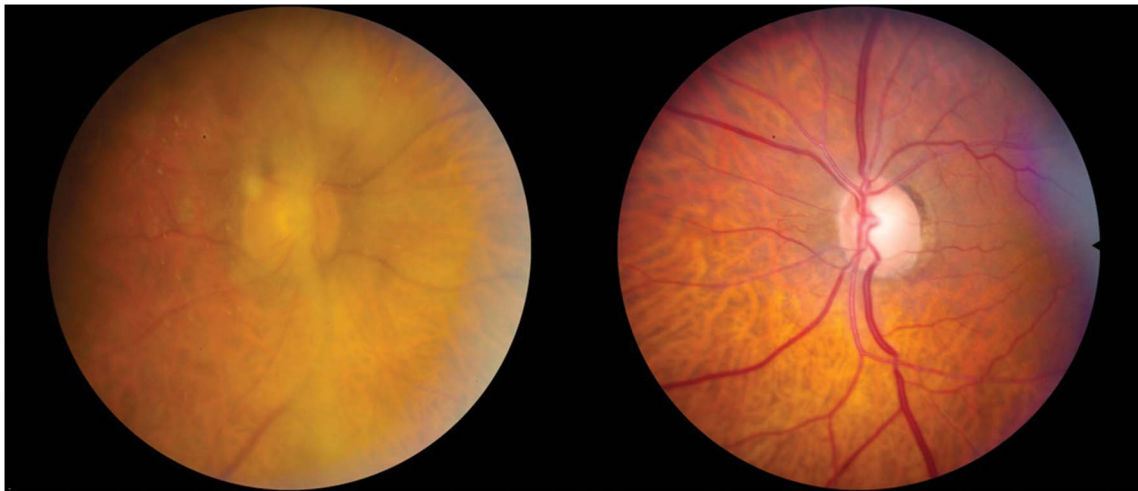
A reduction in signal strength from a media opacity or optic nerve edema can result in loss of retinal layer features, intraretinal hypodensity, and artifacts in layer segmentation and interpretation. The most common causes of media opacity which reduce signal strength and compromise retinal layer

segmentation are dry eye, corneal opacities, cataract, and vitreous opacities. There is a mild decrease in the segmented RNFL thickness associated with decreasing signal strength (20–22). Vizzeri et al (22) found a positive linear relationship between signal strength and mean RNFL thickness among healthy patients analyzed with Stratus OCT (Carl Zeiss Meditec). It was found that for each unit of decrease in signal strength, the average RNFL thickness had a corresponding decrease of 2 μm. In addition, improper alignment of the scan on the retina could introduce variability in repeat scans and changes in sectoral RNFL thickness, mostly through horizontal shifts of the scan placement (22,23). Once signal strength drops below a value of 7 (10 being maximum) in the Cirrus platform, the segmentation algorithm can sometimes fail and produce large regional errors in the derived RNFL thickness (Fig. 1). Other OCT platforms have similar signal strength measurements. Focal media opacities, such as posterior vitreous detachment and hemorrhage, can cause a focal loss of signal strength giving a false appearance of local areas of RNFL drop out that can lower the average RNFL thickness or artificially create segmental areas of thinning.

In addition to media opacity, edema of the retina can have a large effect on the signal strength of the layers under it and hence the accuracy of segmentation by OCT. For example, optic nerve head edema will block the ability to find the full extent of the underlying Bruch's membrane and its termination at the neural canal opening, which can affect the accuracy of the disc area being reported and make it appear larger than its true size (Figs. 2, 3).

Significant disc edema will also make segmentation inaccurate due to distortion of the retinal layers by edema (Figs. 2–4). Failed segmentation can often be identified as rectangular-shaped areas of absolute loss in the Cirrus RNFL deviation map that do not follow the normal arcuate pathway of the RNFL (Fig. 2). Careful inspection of the B scans allows this artifact to be recognized. While the Spectralis OCT analysis of the nerve does not currently display a RNFL deviation map, errors in segmentation of the RNFL can be seen by inspecting the B scan (Fig. 4). Errors in segmentation can also be seen by examining the TSNIT (temporal-superior-nasal-inferior-temporal) RNFL thickness plot, which is available on most commercially available OCT displays (Figs. 2–4). A RNFL thickness approaching 0 μm on the TSNIT RNFL thickness plot can only be due to segmentation error because prior studies have shown that the RNFL thickness can only drop to approximately 30–40 μm despite long-standing optic neuropathies with no light perception vision because of residual glial cells, retinal blood vessels, gliosis, and nonfunctioning ganglion cell axons that contribute to the RNFL (24,25).

A prominent vitreoretinal interface opacity can also cause errors in segmentation of the RNFL thickness (Fig. 4). All OCT algorithms attempt to identify the internal limiting membrane as the upper boundary of the RNFL. Occasionally a prominent vitreous opacity will be incorrectly identified as
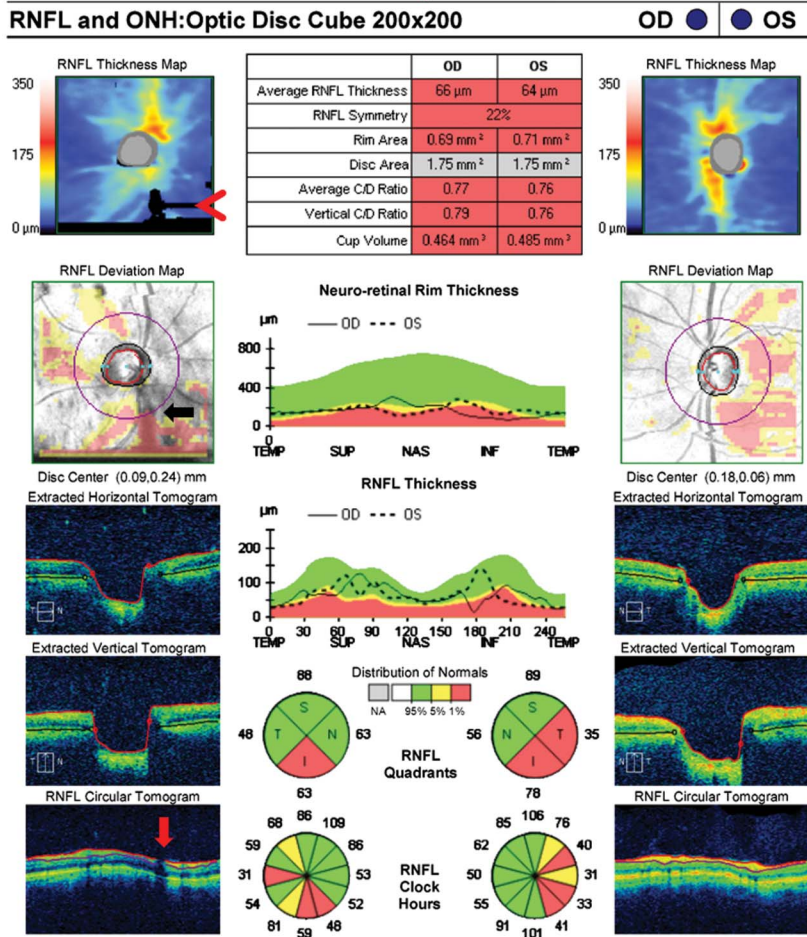
FIG. 1. A reduction in signal strength can result in loss of retinal layer features and introduce artifact in the RNFL analysis. This patient has normal tension glaucoma, left eye > right eye, and asteroid hyalosis in the right eye (upper left image) that has reduced the signal strength to 6/10 (*red arrow*). This causes an inferior regional error of segmentation of the RNFL thickness, which can be seen as black rectangular areas of absolute thinning on the RNFL thickness map (*red arrowhead*). Only a small portion of this segmentation error intersects the RNFL circular scan and has an effect on the RNFL thickness (RNFL deviation map, *black arrow*), which can be seen as a disruption of the normal segmentation on the RNFL circular tomogram (*red vertical arrow*). This causes an artificially low inferior quadrant RNFL thickness in the right eye, especially at the 5 o'clock position. RNFL, retinal nerve fiber layer.
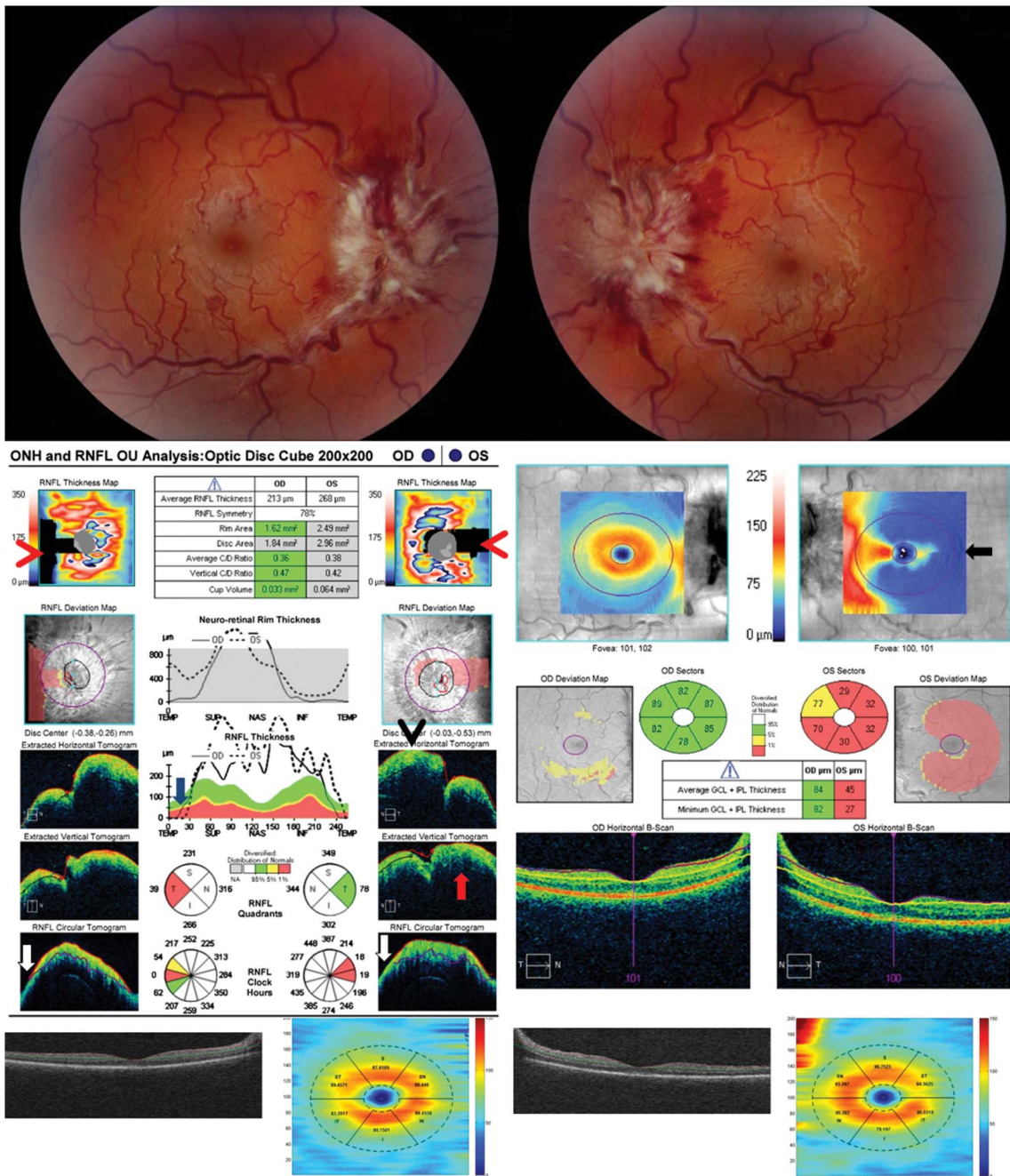
FIG. 2. Significant optic disc edema will cause errors in segmentation on OCT due to distortion of the retinal layers surrounding the optic nerve. This patient presented with Frisen-grade 4 papilledema in both eyes from idiopathic intracranial hypertension (upper images), which led to errors in measuring disc area, rim area, and RNFL thickness on OCT (middle left). The disc area is artificially enlarged in the left eye because the termination of Bruch's membrane is obscured by the edema and cannot be correctly identified as seen in the B scan (*red arrow*). The RNFL thickness is underestimated because of the incorrect segmentation of the temporal RNFL in both eyes and a small portion of the nasal RNFL in the left eye, which is apparent as absolute defects (*black rectangles*) within the RNFL thickness map that do not follow the anatomical distribution of the RNFL arcuate bundles (*red arrowheads*). This occurs because of a decreased ability to accurately segment the layers due to the disc edema (temporal RNFL, both eyes, *white arrows*) and decentering of the RNFL data on the z-axis resulting in truncation of the scan, which can be seen on the B scan (nasal RNFL, left eye, *black arrowhead*). A nonphysiologic decrease in the RNFL thickness to 0 μm temporally on the RNFL temporal-superior-nasal-inferior-temporal thickness plot can be seen in both eyes (*blue arrow*). In addition, the disc edema causes an error in segmentation of the GCL-IPL complex in the left eye (middle right, *black arrow*). Note the unusual distribution of the GCL-IPL thickness on the color map of the left eye, providing a clue that the algorithm is failing. The Iowa Reference lgorithm, which utilized 3-dimensional information, shows accurate segmentation of the GCL-IPL complex of both eyes (lower images). OCT, optical coherence tomography; RNFL, retinal nerve fiber layer.

the internal limiting membrane, which will result in an artifactually thickened RNFL measurement.

Errors in segmentation of the RNFL also can occur from decentering of the scan in the z-axis, which can cause truncation of the image, resulting in areas of absolute loss on the RNFL thickness plot. This is particularly a problem in patients with significant disc edema, tilted optic nerves, or significant cupping because the peripapillary RNFL may be difficult to capture on a single B scan due to the differences in height between the opposite sides of the circular RNFL scan (Figs. 2, 3, 5). Examination of the B

scans will demonstrate an area of the scan that is truncated. This artifact can be reduced by ensuring that the data are well centered on the z-axis during acquisition.

Effects of Refractive Error and Axial Eye Length on the RNFL Thickness

Above average axial eye length, typically associated with high myopia, is associated with a thinner RNFL compared to the normal population. This is important because the normal population database used by the manufacturer specifically excludes subjects with a high refractive error
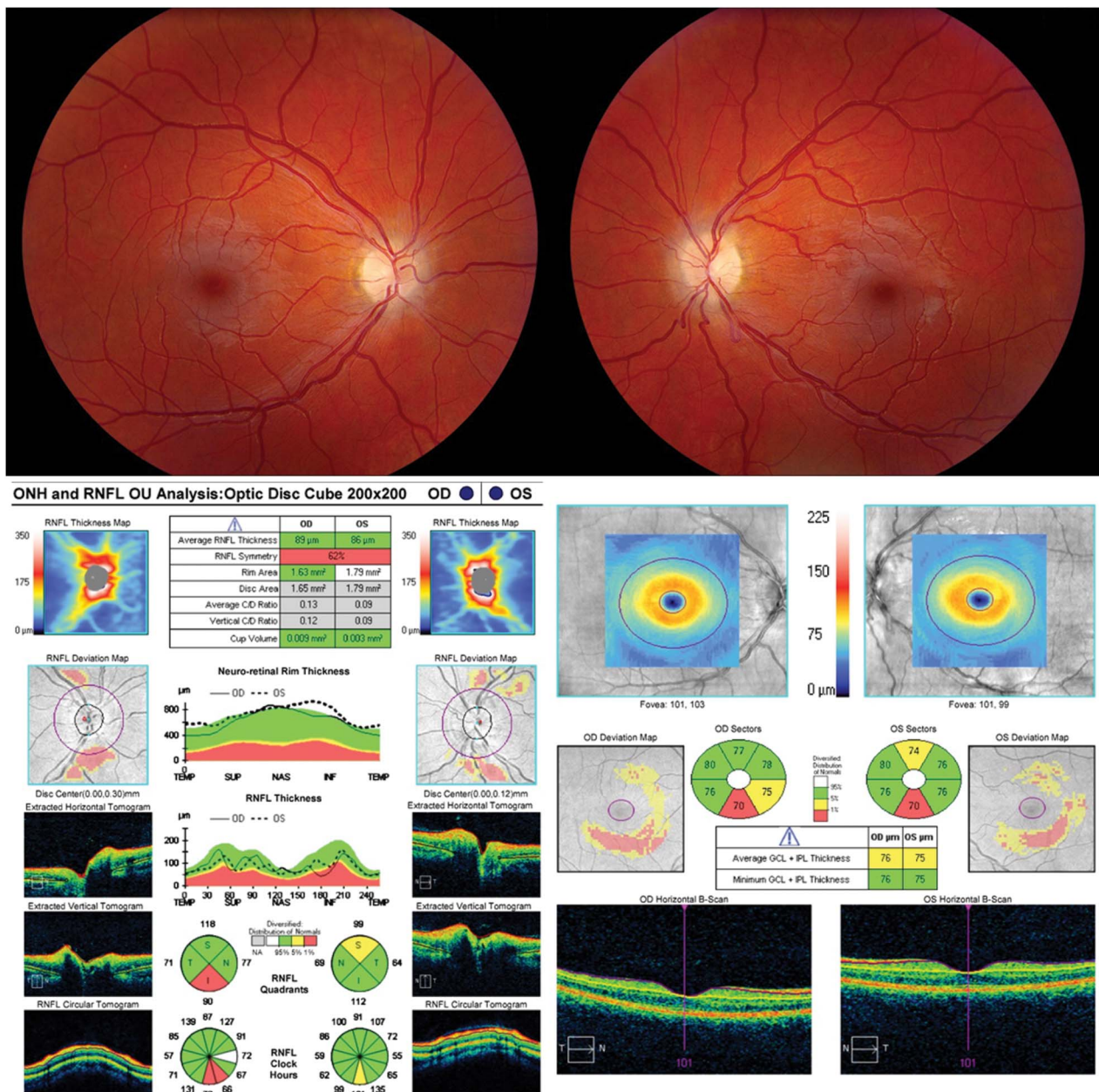

FIG. 3. OCT 3 months after medical treatment for IIH of patient shown in Figure 2 now shows accurate segmentation of the RNFL, disc size, and GCL-IPL with some residual loss of the RNFL and GCL-IPL thicknesses. GCL-IPL, ganglion cell layer-inner plexiform layer; OCT, optical coherence tomography; RNFL, retinal nerve fiber layer.
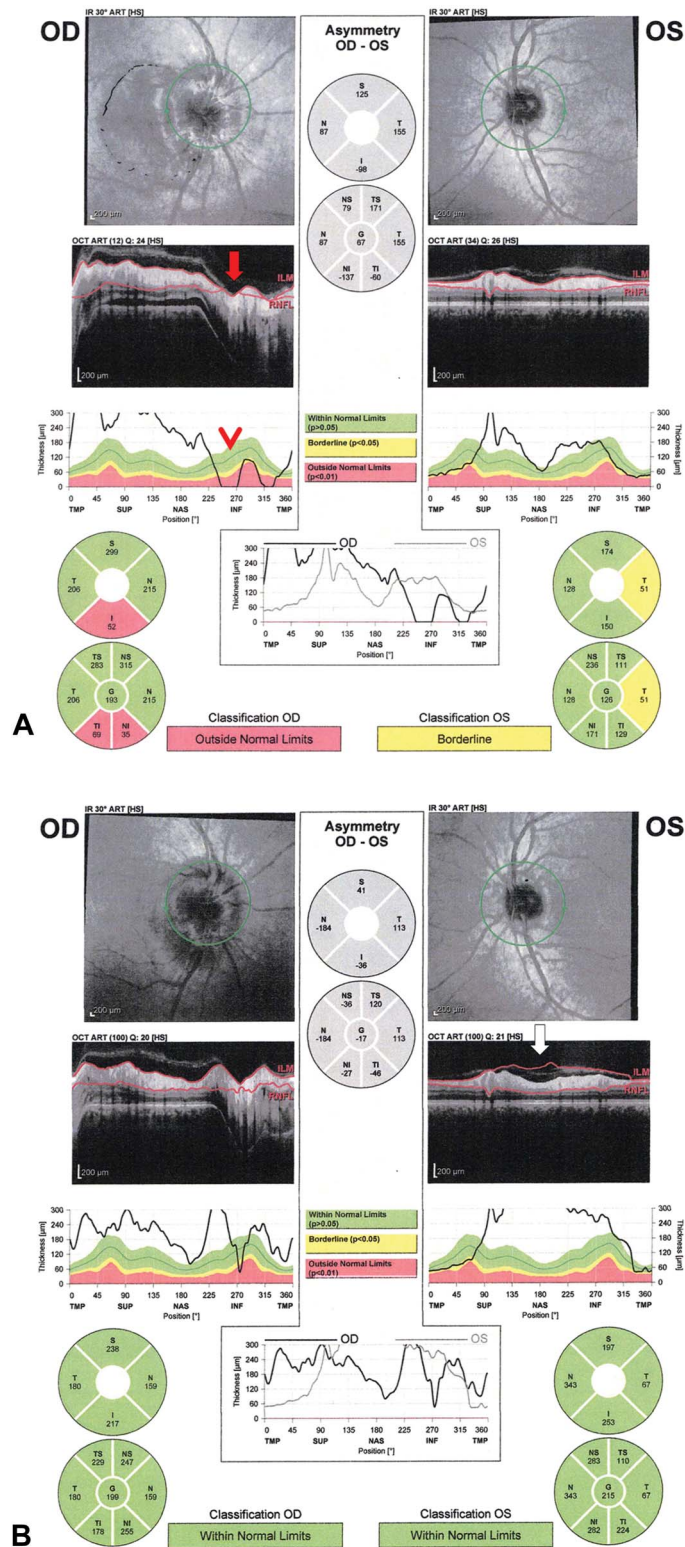
FIG. 4. Spectralis OCT with artifacts in the RNFL thickness. **A**. this patient presented with bilateral asymmetric papilledema with Frisen-grade 3 disc edema of the right optic nerve and very mild disc edema of the left optic nerve. Segmentation error of the RNFL is seen on the B-scan of the right eye (*red arrow*), which causes a nonphysiologic decrease in the RNFL thickness toward 0 μm inferiorly on the RNFL temporal-superior-nasal-inferior-temporal thickness plot (*red arrowhead*). **B**. A repeat OCT 1 month later shows less segmentation artifact of the RNFL in the right eye. However, the left eye at 1 month shows a significant thickening RNFL thickness due to errors in identifying the internal limiting membrane due to prominent vitreoretinal interface opacity, which can be seen on the B-scan (*white arrow*). OCT, optical coherence tomography; RNFL, retinal nerve fiber layer.
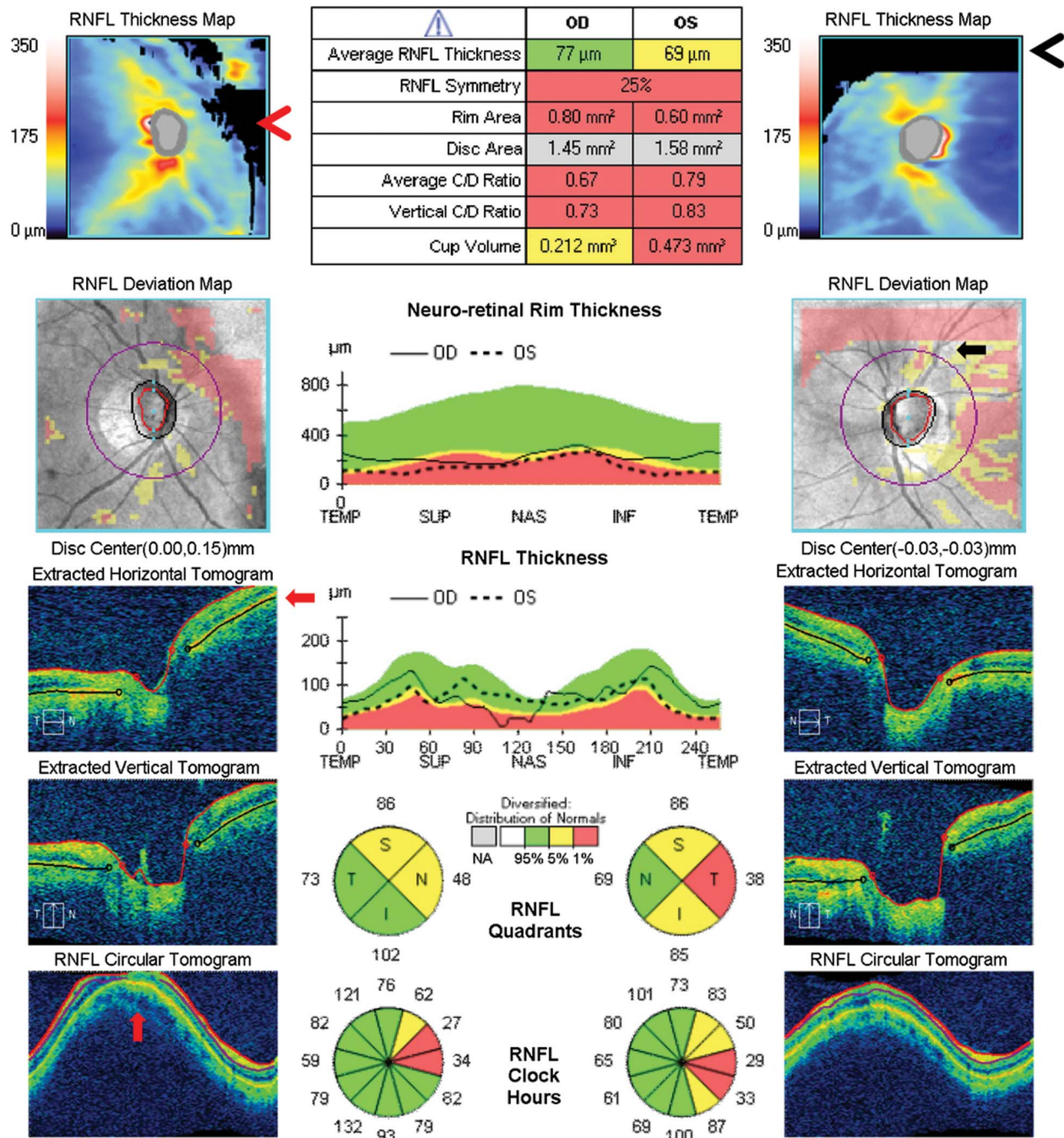
FIG. 5. Truncation of RNFL data due to decentering on the z-axis. This patient has primary open-angle glaucoma in the left eye and is a glaucoma suspect in the right eye. Displacement of the scan along the z-axis (decentering) causes the nasal portion of the inner retina to be truncated in the right eye (B scan and RNFL circular tomogram in lower left panel, *red arrows*). This results in regional errors in the derived RNFL thickness, which can be seen as irregular black rectangular areas of absolute thinning on the RNFL thickness map (*red arrowhead*). This truncation of the data causes an artificially low RNFL thickness in the superior and nasal quadrants in the right eye. The left eye also has areas of superior artifactual absolute thinning on the RNFL thickness map (*black arrowhead*) from z-axis truncation, but is not seen on the B scans and does not affect the measured RNFL thickness because the scan circle around the optic nerve does not encompass this area of artifact as can be seen on the RNFL deviation map (*black arrow*). Both eyes are predisposed to this z-axis truncation because of the presence of a mild posterior staphyloma. RNFL, retinal nerve fiber layer.

(usually encompassing spherical equivalent between -5.00 and +5.00). In addition, the effect of large refractive errors and associated long or short axial eye length may go unrecognized in patients who have undergone refractive surgery or cataract extraction with intraocular lens implantation.

Patients with myopia have an increased risk of developing glaucoma (26), and, therefore accurate measurements of the RNFL are important. The ability to detect glaucomatous optic neuropathy in myopic patients by RNFL measurements is more difficult compared to emmetropic patients (27). There are multiple studies showing that the average peripapillary RNFL thickness decreases with myopic refractive error and increased axial eye length, while the disc area is underestimated (Fig. 6) (16,28–35). In addition, patients with hyperopia and shorter axial eye lengths show an increase in RNFL thickness and an overestimation of optic disc area on OCT (31). These findings are attributed to ocular magnification effects of axial eye length, except in pathological myopia, where true retinal thinning may be present. When adjusting for ocular magnification, the negative correlation between these OCT measurements and both axial eye length and refractive error is lost (28,31,36). In fact, the average corrected RNFL thickness and optic disc area may increase with increasing axial eye length when ocular magnification is taken into account (28,36). The finding of a truly larger optic disc area with high myopia and smaller optic disc size with high hyperopia is found with analysis of fundus photos as well (37,38).

The association between refractive error and changes in optic nerve head size and RNFL thickness in OCT measurements is entirely attributed to axial length-induced ocular magnification, rather than any effects of refractive error itself. There is a correlation between spherical equivalent and these parameters, but this is due to the strong correlation between refractive error and axial eye length. Prior studies have demonstrated no change in RNFL thickness after refractive surgery for myopia (31,39,40). However, because of the strong correlation between refractive error and axial eye length, high refractive error can be used as a surrogate for an abnormal axial eye length to determine if there is likely a significant ocular magnification error introduced in the OCT measurement. For example, Kang et al (28) found that in eyes with ≥4 diopters of myopia, the mean circular peripapillary scan magnification was increased to greater than 5%. This would significantly underestimate the true RNFL thickness and optic nerve head measurement in high myopes (28). Because the effects of axial-length magnification remain in patients that are postrefractive surgery and pseudophakic, they may be unrecognized and lead to incorrect interpretation of the OCT if their axial eye length is not known.

Because most current OCT machines do not account for ocular magnification, patients with long or short axial eye lengths will have artificially low and high OCT measurements respectively, when compared to the normative database. If the axial eye length is known, the OCT measurements can be corrected with the modified Littmann formula as described by Bennet et al (41). In the future, a normative database stratified by axial length may be helpful to compare patients with high refractive error. In addition, future OCT machines may provide the ability to measure axial eye length and account for ocular magnification while obtaining measurements.

Association of Refractive Error and Axial Eye Length on the Angular Distribution of the Retinal Nerve Fiber Layer Bundles

In addition to the changes in the overall RNFL thickness, the peaks on the TSNIT (temporal-superior-nasal-inferior-temporal) RNFL thickness plot are shifted temporally toward the fovea in myopes compared to the general population (Fig. 6) (28,42–47). This is due to the developmental association of axial myopia or hyperopia with the regional distribution of the superior and inferior arcuate nerve bundles. With increasing myopia, there is an increase in prevalence of a more temporal angle of the arcuate nerve bundles as they enter the nerve head, while increasing hyperopia is associated with a more vertical angle of the entrance of the arcuate bundles into the optic disc. Due to the more temporal shift of the RNFL peaks in myopia, the temporal RNFL thickness may be elevated, while the superior and inferior RNFL thickness may be reported as decreased in myopic patients when compared to the average arcuate bundle distribution of a normative database (28,34,35,43,44,46,47). A similar situation occurs with hyperopic eyes in which the more vertical angle of the arcuate bundles results in a probability plot returning abnormal RNFL thickness in the location of the expected normal arcuate bundle locations. While the overall average thickness of the RNFL is dependent on axial length-induced ocular magnification, the correlation between myopia and temporal shift of the RNFL peaks and its associated changes in RNFL thickness does not normalize when ocular magnification is taken into account (28,31).

The cause for the more temporal location of the RNFL peaks in myopia is still not entirely understood. It has been speculated that there may be temporal dragging of the retina during development secondary to a long axial eye length or from the temporal optic disc tilt that is seen in myopia (28,34,42,44). Others have proposed that the temporal shift of the RNFL peaks compared to the more emmetropic population may be due to the OCT images taken at a more oblique angle because of the tilted nature of the discs in many high myopes (44,48). Interestingly, it has been shown that both the arcuate RNFL peaks and retinal arteries are shifted temporally in myopes and that the angular distribution of the RNFL peaks has a stranger correlation with the position of the retinal arteries than with the axial eye length (46). The correlation between the RNFL peaks and the arteries are thought to arise from 2 primary mechanisms. First, the arteries themselves contribute to thickening of the RNFL. Hood et al (49) approximated 13% of the overall OCT measured RNFL thickness is directly due to the added contribution from blood vessels within the RNFL. This effect may be most apparent on
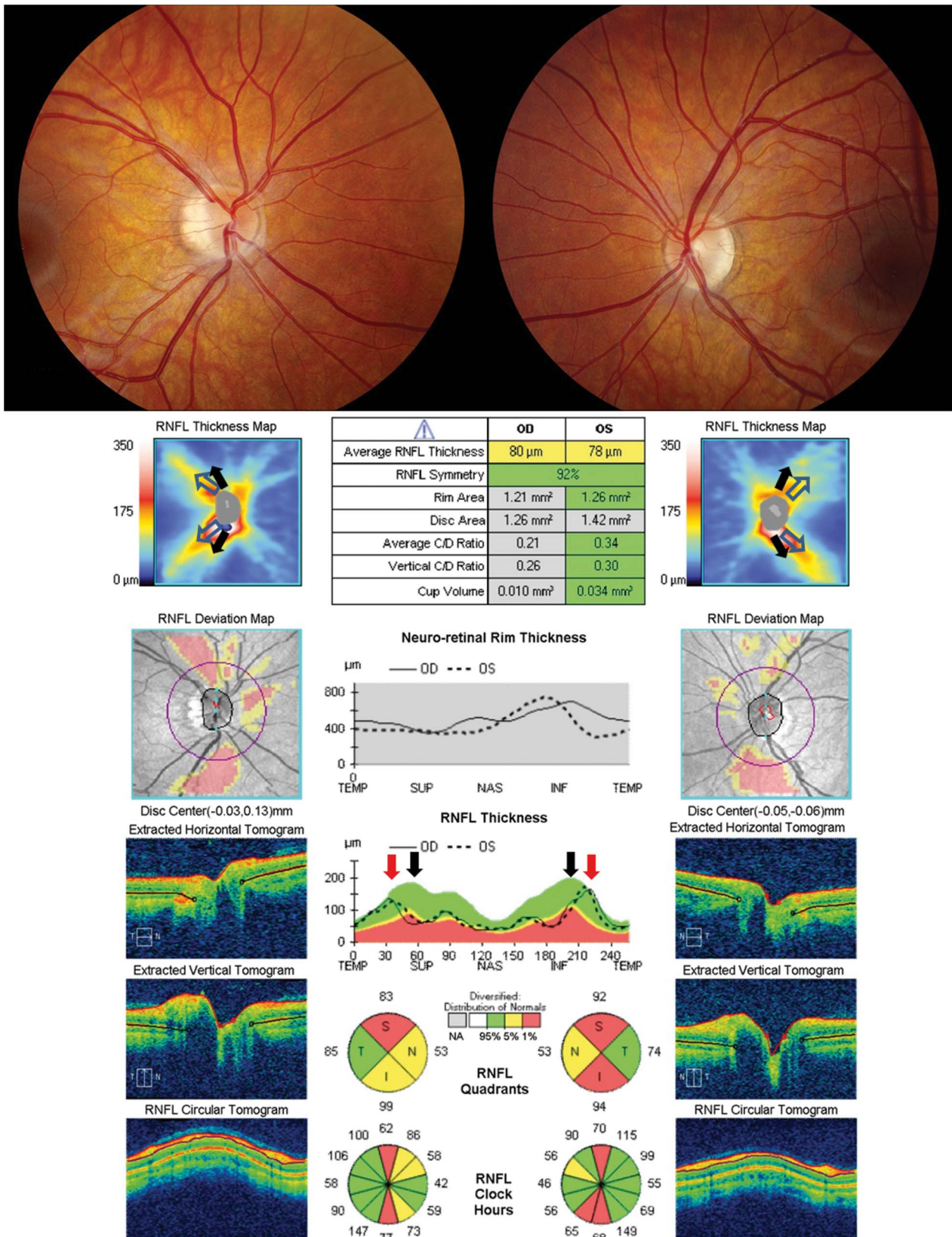
FIG. 6. Myopes with long axial eye lengths have a decrease in the image size due to ocular magnification effects leading to a smaller measured disc size and an underestimation of the RNFL thickness. In addition, myopes with long axial eye lengths often have blood vessels and the RNFL arcuate bundles deviated more temporally compared to a normal eye, which causes

(continued)

Cirrus- and Stratus-derived RNFL thicknesses where the blood vessel contours are smoothened and, therefore, directly contribute to the measured RNFL. Conversely, in other OCT machines, such as Spectralis, the blood vessels appear as individual humps on the RNFL profile and probably contribute less to the measured RNFL thickness. Second, the spatial pattern of axon distribution can signal the direction of blood vessel distribution within the retina development and branches of the central retinal artery appear to spatially correlate with the thickest bundles of axons (49–51). Therefore, the distribution of the retinal arteries can be used to identify patients that may have RNFL peaks in an anomalous location.

When evaluating for optic neuropathy, these shifts in the RNFL peaks are important to acknowledge because they can lead to false-positive or false-negative results when interpreting the RNFL profile relative to the expected profile in normal eyes. The temporal shift of the RNFL peaks in myopes could lead to the incorrect interpretation of a superior and inferior arcuate bundle defect in an eye that is normal or could obscure true pathology within the temporal RNFL bundle. The macular GCL-IPL complex may be more immune to these artifacts and therefore may be used to better evaluate optic neuropathy in a patient with large deviations in the pattern of RNFL peaks compared to normal eyes (52). In addition, shifts in the RNFL peaks can help identify patients that have large differences in axial eye length that can be associated with thinner or thicker average RNFL as discussed above. This is especially important in interpreting OCT scan in patients that are pseudophakic or postrefractive, when the axial eye length is not known.

Effects of Cyclotorsion on the Distribution of the Retinal Nerve Fiber Layer Bundles

Cyclotorsion of the eyes for any number of reasons (including head tilt) will cause an apparent change in the profile of the superotemporal RNFL thickness and the inferotemporal RNFL thickness, with respect to the pattern of the normative database RNFL TSNIT OCT profile (Fig. 7). This shift of the peaks will lead to false-positive probability plots of both TSNIT and RNFL map when compared to the normative database. Hwang et al (53) found that voluntary head tilt among normal healthy subjects introduced these changes on the RNFL when measured with Cirrus OCT. In a study by Valverde-Megias et al (54), the fovea location was shifted on Spectralis OCTs obtained from both healthy adults and patients with glaucoma to mimic

poor foveal fixation and found that the induced torsion caused a displacement of the peaks and valleys of the RNFL profile and introduced changes in the probability charts. Spectralis OCT software attempts to correct for apparent ocular torsion or head tilt by placing scans on the retina during acquisition in parallel to a line connecting the fovea to the disc or rotated in the case of circular scans to account for apparent distortion. However, it has also been determined that there can be true displacement of the fovea with respect to the nerve head as a developmental variation in normal eyes (55). Correcting for it in such cases will introduce an error in the profile of the distribution of retinal nerve fiber bundles. We have recently noted that cyclotorsion from motility abnormalities, such as skew deviation or fourth nerve palsy, will also introduce shifts in the RNFL peaks and cause false positives and localized areas of artifactual thinning when compared with the normative database on the TSNIT and RNFL maps (56). Interestingly, the amount of shift of the peaks correlated with the expected cyclotorsion based on clinical measurements and fundus photography, allowing the amount of displacement in the superotemporal and inferotemporal RNFL bundles on OCT to be used to measure the amount of torsion (Fig. 7).

Peripapillary Atrophy

Peripapillary atrophy may, in some cases, interfere with the segmentation of the RNFL although this occurred mostly with segmentation algorithms of time-domain OCT, such as Stratus OCT. When this took place, it was usually due to the inability of the segmentation software to accurately align and register the A scans along the retinal pigmented epithelial border, which adversely affects segmentation of the retinal layers (57). This is clinically important because peripapillary atrophy is found more commonly in glaucomatous patients. Jonas et al (58) found β-zone peripapillary atrophy in 62.4% in primary open-angle glaucoma patients and 84% in normal tension glaucoma patients compared to 15% among normal patients. Fortunately with the advent of newer spectral domain OCT, the inaccuracy of segmentation caused by peripapillary atrophy with time-domain OCT is markedly reduced (57).

Artificial Increase in Retinal Nerve Fiber Layer Thickness

Gliosis of the optic nerve and retinal axons following optic nerve damage can result in an increase in RNFL thickness despite significant atrophy of axons. In such cases, the macular GCL-IPL complex will show atrophy while the peripapillary

an increase in the temporal RNFL thickness and a decrease in the superior and inferior RNFL thicknesses. This patient is a −8D myope and has an artifactually low RNFL average thickness. In addition, the RNFL peaks and arteries are shifted temporally resulting in thinning of the superior and inferior RNFL thickness analysis. The superior and inferior arcuate bundles (*green open arrows*) are more temporally displaced on the RNFL thickness maps compared to a normal patient (*black arrows*). The temporal shift of the RNFL peaks can also be seen by examining the temporal-superior-nasal-inferior-temporal RNFL thickness profile plot and comparing the superotemporal and inferotemporal peaks of both eyes (*red arrows*) to the normal population shown in green (*black arrows*). Note how the shift in location of the peaks causes apparent abnormal red areas (less than or equal to the first percentile of normal) in the probability maps and sector plots. RNFL, retinal nerve fiber layer.
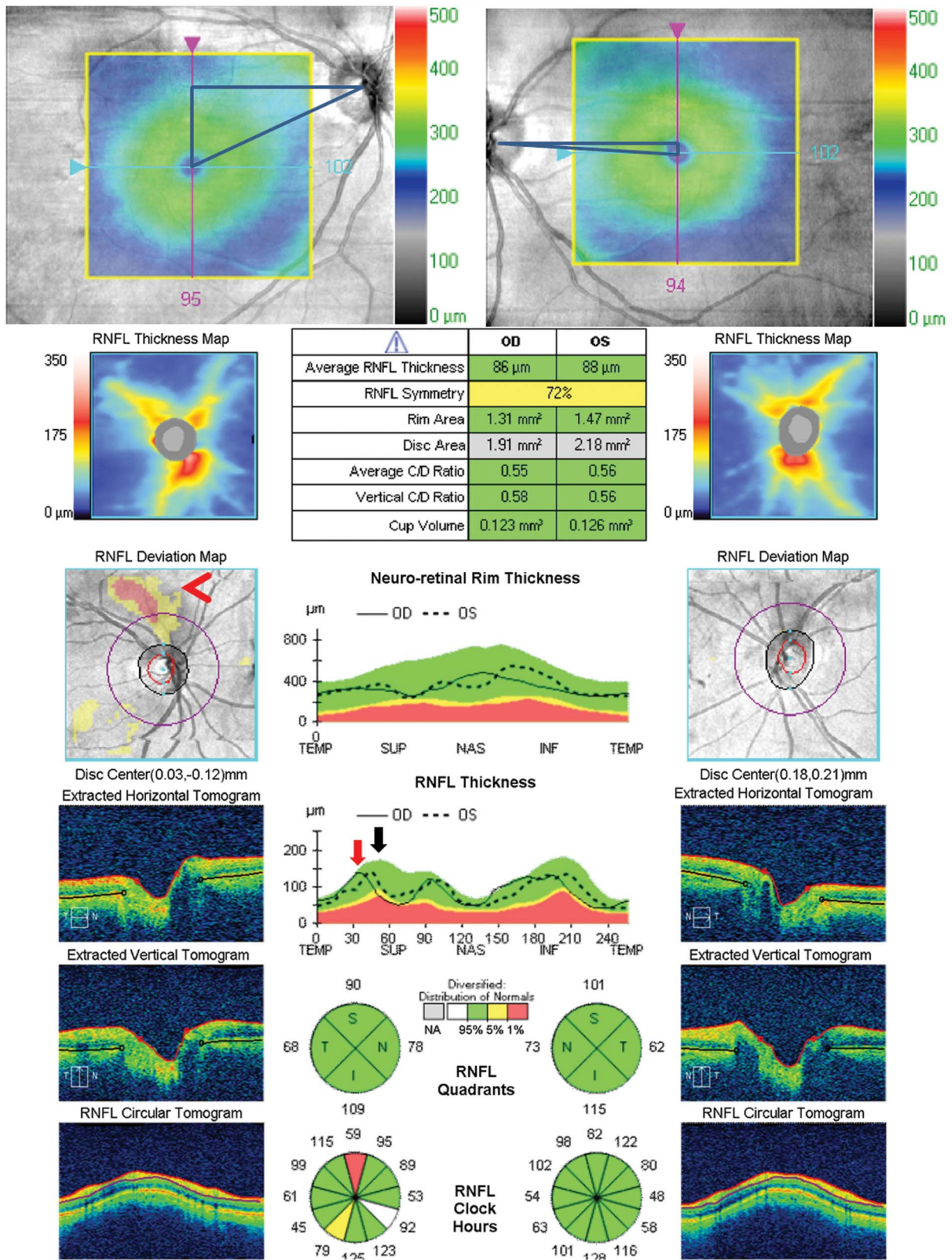
FIG. 7. Cyclotorsion of the eyes will introduce a shift of the RNFL peaks with respect to the normative database RNFL TSNIT profile that can lead to false-positive probability plots of both TSNIT and RNFL when compared to the normative database. This patient had a right fourth nerve palsy causing significant excyclotorsion of the right eye, which was measured at 17° on double (*continued*)

RNFL can be thickened due to the gliosis (Fig. 8). The presence of a myelinated nerve fiber layer can also lead to an increase in RNFL thickness that can lead to an overestimation of the number of axons in the corresponding location (Fig. 9). Acute edema of the inner retina due to artery occlusions can cause an increase in RNFL thickness associated with a hypodensity in the outer retina due to signal attenuation in this layer. Epiretinal membranes, if present, are usually incorporated into the segmented RNFL and can cause an artificial increase in RNFL thickness that can obscure pathologic loss of axons (14).

Interindividual Differences in the Thickness of the RNFL in Normal Eyes

Because patients are compared against a normal population-derived probability plot, individuals who are born with a greater or lesser thickness of their RNFL may cause an underestimation or overestimation of acquired axon loss based solely on the probability plot. Interocular asymmetry may help overcome this in cases of unilateral disease (Fig. 10). In addition, temporal and nasal bundles are normally thin relative to the arcuate bundles and their thickness can vary between normal subjects; this makes it more difficult to detect significant thinning in the temporal and nasal clock-hour sectors based on the probability plot. Because of the RNFL in the papillomacular bundle is normally thin and varies among individuals, it takes a large amount of damage and thinning for this layer to drop between the normal range. Compounding this problem is that the RNFL has a small dynamic range of potential thickness. In contrast, the retinal ganglion cell layer is thickest in the macula where the soma is located, which corresponds to the temporal RNFL bundle due to multiple layers of retinal ganglion cells. This explains why the ganglion cell-inner plexiform layer (GCL-IPL) complex is thickest in the macula, has a larger dynamic range than the RNFL in the papillomacular bundle, and provides a more sensitive measure of neuronal loss in the papillomacular bundle.

Optical Coherence Tomography Interpretation of Optic Disc Area, Rim, and Cup

The determination of the disc area by its borders is defined by OCT using the termination of Bruch membrane and is subject to inaccuracies when the signal strength at this location is reduced. This may occur in the setting of media opacities and also with different causes of disc edema, including papilledema, acute anterior ischemic optic neuropathy (AION), and pseudopapilledema (with or without drusen). This can cause the segmentation algorithm to report a disc area larger than its true size because the termination point of Bruch membrane and its termination at the neural canal opening is inaccurately located more proximally by the software due to loss of signal and structural features at its distal location, bordering the neural canal (Figs. 2, 3). Averaging of B-scans during image acquisition and the use of enhanced depth penetration can improve signal strength and increase segmentation accuracy of the neural canal and hence, disc area.

The determination of rim location and rim area is determined by segmentation software, which finds the location along the inner retinal surface of the cup that is the shortest distance from the end of Bruch membrane. Therefore, errors in determination of the border of the neural canal (disc area) will adversely affect the determination of the rim location because it is relative to this measurement (Figs. 2, 3).

Determination of the cup-to-disc ratio not only depends on correct segmentation of the disc border, but also on the size of the optic disc. Subjects who are born with large neural canals (large discs, including megalopapilla) and small neural canals (small discs, including optic nerve hypoplasia) that are outside the normative range may cause inaccurate designation of an abnormal cup. For example, a small optic nerve will appear congested and have nasal elevation of the disc, often referred to as a "little red disc," and can be mistaken for disc edema (59). OCT analysis of the nerve demonstrating a small disc diameter with a normal RNFL thickness can help differentiate pseudopapilledema from true papilledema (Fig. 11). Alternatively, a large optic disc can lead to a large cup-to-disc ratio that may not be pathologically acquired and may represent physiological cupping (Fig. 12). As a consequence, patients labeled as glaucoma suspects based on their large cup-to-disc ratio may be more accurately diagnosed as normal if their optic disc area is shown to be larger than normal based on the OCT-derived measurement.

MACULAR GANGLION CELL-INNER PLEXIFORM OPTICAL COHERENCE TOMOGRAPHY ANALYSIS

### Macular Ganglion Cell-Inner Plexiform Layer Thickness

OCT segmentation algorithms have recently instituted segmentation of the retina GCL-IPL layer complex within the macula. The ganglion cell layer contains the cell bodies that give rise to the axons that make up the RNFL and optic nerve. Thinning of the GCL-IPL layer in the macula has

Maddox rod. The excyclotorsion of the right eye can be seen on the OCT macular thickness map superimposed on the OCT fundus image and can be quantified by triangulation (top images). This introduced an artifactual superior arcuate area of thinning on the probability map with respect to the normative database (*red arrowhead*) because of the temporal shift of the superotemporal peak, which can also be seen on the TSNIT plot (*red arrow* indicates shifted peak, *black arrow* indicates the normal location of the superotemporal peak). In addition, the magnitude of the shift of the peak compared to the normative database equaled the amount of excyclotorsion measured by triangulation on the fundus photo and clinically on double Maddox rod. OCT, optical coherence tomography; RNFL, retinal nerve fiber layer; TSNIT, temporal-superior-nasal-inferior-temporal.
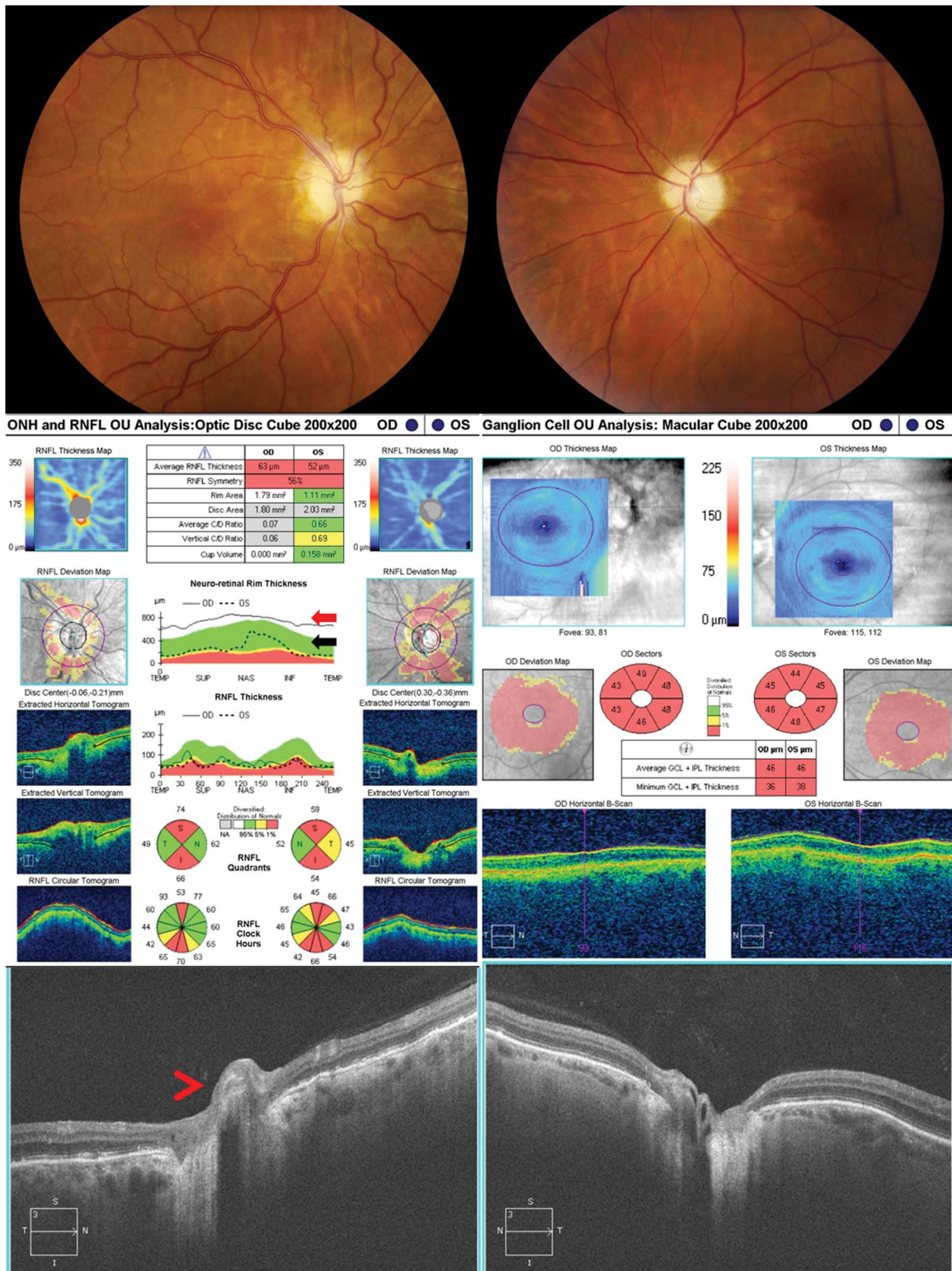
FIG. 8. Artificially increased RNFL thickness from gliosis of the nerve. This patient has no light perception, right eye and 20/400, left eye, secondary to bilateral orbital apex/cavernous sinus meningiomas. Despite worse vision in the right eye, the RNFL thickness is greater in the right eye compared to left eye secondary to optic nerve gliosis (although both show thinning of the RNFL). The gliosis of the right optic nerve causes the neuroretinal rim to be thicker (*red arrow*) than the general population (*black arrow*). In addition, the B-scan through the right optic nerve shows an elevated optic disc with no cup because of the gliosis (bottom image, *red arrowhead*). The extent of the damage to the right optic nerve is seen in the profound thinning of the macular GCL-IPL thickness. GCL-IPL, ganglion cell layer-inner plexiform layer; RNFL, retinal nerve fiber layer.
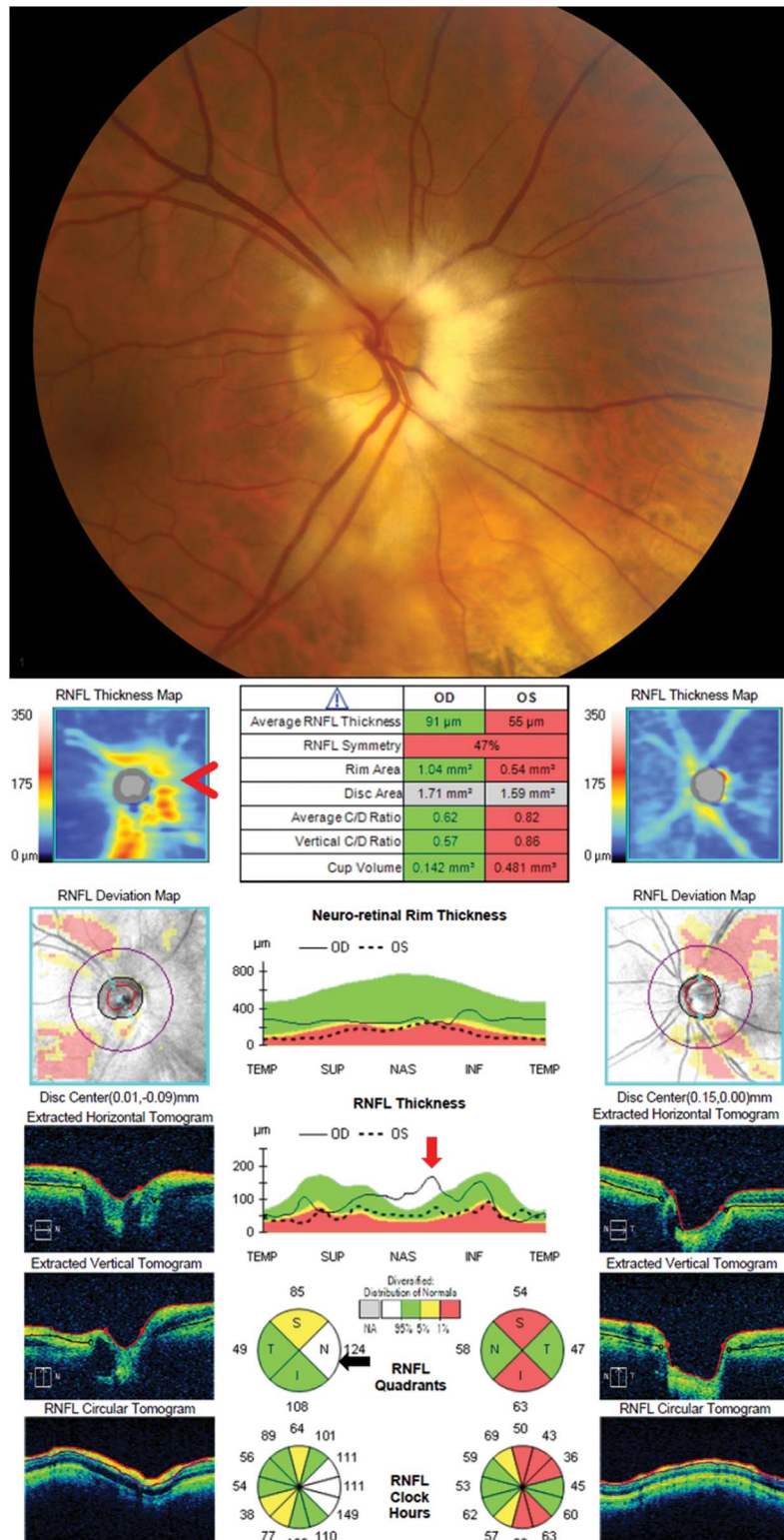
FIG. 9. Artificially increased RNFL thickness from myelinated nerve fiber layer. This patient has primary open-angle glaucoma resulting in optic nerve cupping and thinning of the RNFL. The prominent nasal myelinated nerve fiber layer in the right eye results in a thickened RNFL that obscures thinning of the RNFL from the patient's underlying glaucoma. The RNFL thickness map shows the normally positioned superotemporal and inferotemporal arcuate bundles and also an irregular elevated RNFL nasal to the disc (*red arrowhead*) due to the myelinated nerve fiber layer. The myelinated nerve fiber layer leads to an elevated nasal peak on the temporal-superior-nasal-inferior-temporal plot (*red arrow*), which causes the nasal RNFL thickness to be thicker than the general population and is therefore shown in white on the RNFL quadrant analysis (*black arrow*). RNFL, retinal nerve fiber layer.
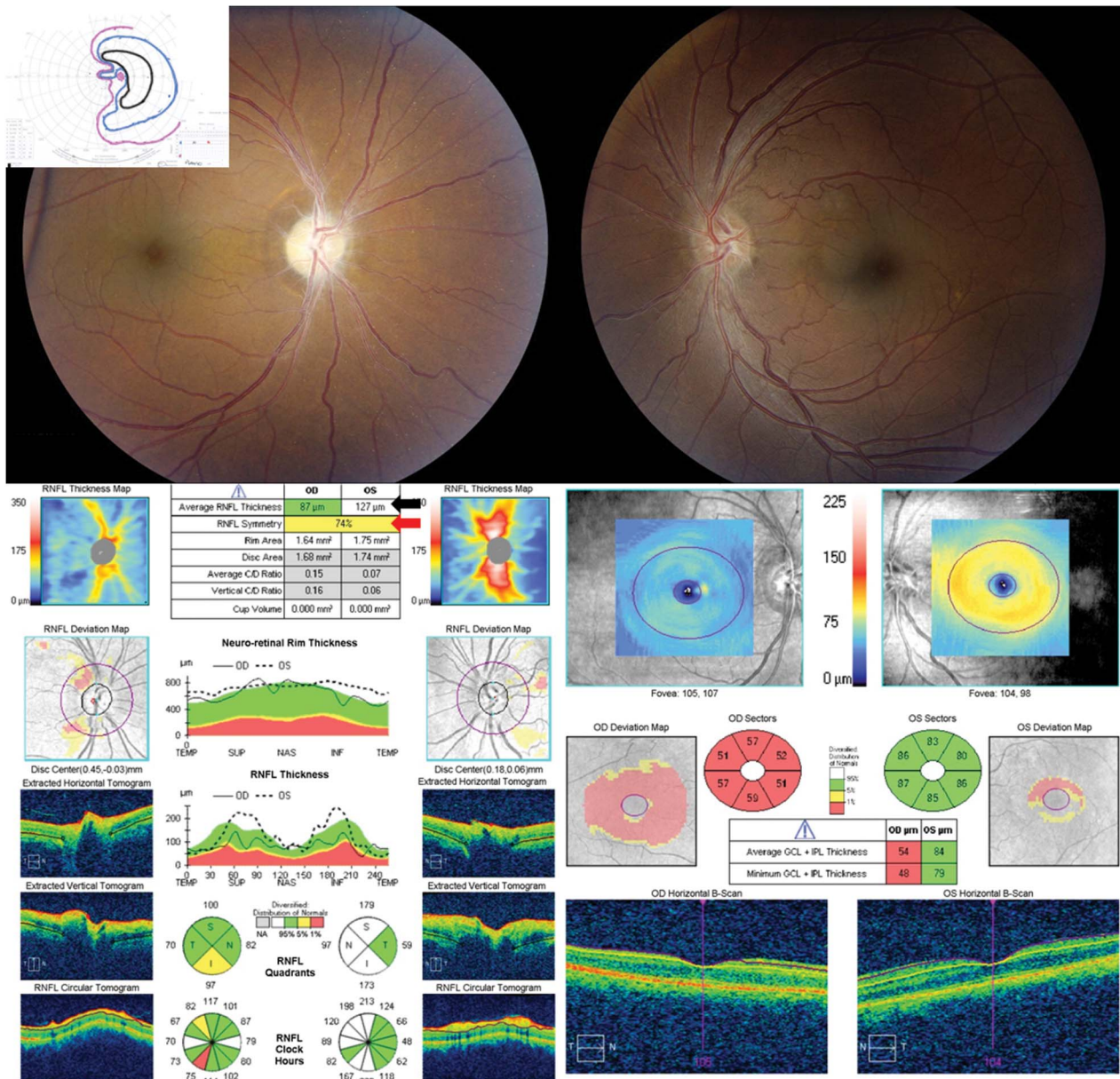
FIG. 10. Interindividual differences in the thickness of the RNFL in normal eyes. This patient suffered nonarteritic ischemic optic neuropathy in the right eye 4.5 months before these photographs. The RNFL in the right eye is still in the normal range compared to age matched control, but 30 microns thinner than the left eye, which was unaffected. This is because his baseline RNFL is thicker than the average population, which masks the thinning of the RNFL in the right eye when compared to the general population. The left unaffected eye has a RNFL average thickness shown in a white box (*black arrow*) and has white filled sectors in the RNFL probability thickness plots (lower left panel) indicating a thickness greater than or equal to the top 5 percentile of normal. The RNFL symmetry analysis can help identify patients with unilateral optic neuropathy (*red arrow*). In addition, the GCL-IPL analysis of the macula demonstrates the severe thinning of the ganglion cell layer in the right eye (lower right image), which correlates with the patient's significant vision loss. GCL-IPL, ganglion cell layer-inner plexiform layer; RNFL, retinal nerve fiber layer.

been found to correlate with visual loss and corresponding loss of visual field sensitivity from optic nerve diseases such as glaucoma, optic neuritis, ischemic optic neuropathy, hereditary optic neuropathy, toxic optic neuropathy, optic nerve glioma, and idiopathic intracranial hypertension (4–12).

Perhaps the most intriguing use of the macular GCL-IPL thickness is in the evaluation of neuronal loss in the presence of optic disc edema. Disc edema and associated increase in RNFL thickness prevent accurate assessment of concomitant axonal loss by OCT due to the significant swollen axons of the optic nerve. This is commonly seen in papilledema or optic disc edema associated with acute and subacute ischemic optic neuropathy and optic neuritis. The problem can be theoretically overcome by analyzing the
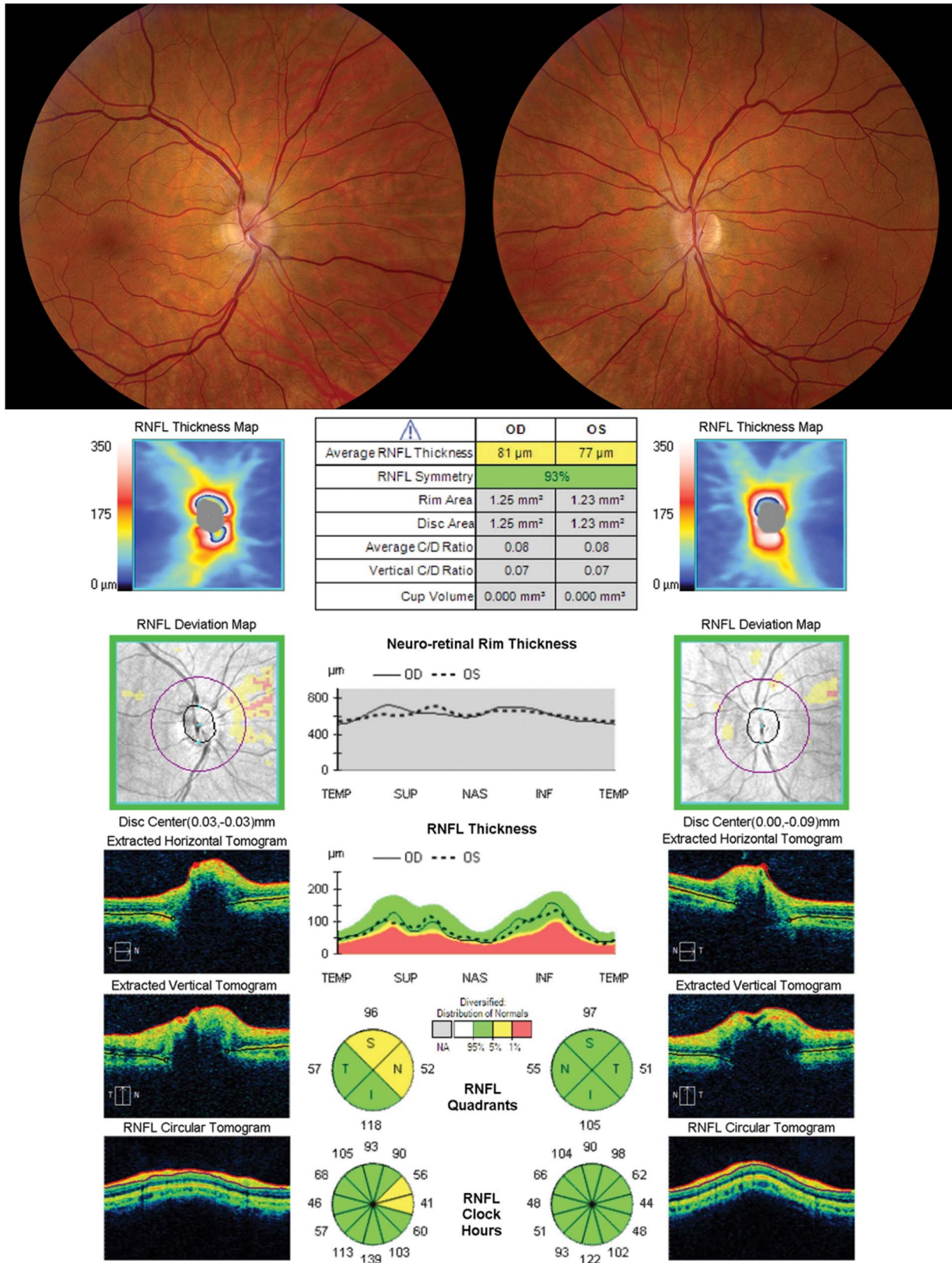
FIG. 11. A small optic nerve can appear elevated nasally and give the appearance of optic disc edema. This patient was referred for evaluation of possible papilledema. Fundus photography demonstrates small optic discs with nasal elevation, without obscuration of the vessels. OCT of the optic nerve demonstrates a small disc area and a normal RNFL thickness in both eyes, confirming the suspicion for pseudopapilledema. OCT, optical coherence tomography; RNFL, retinal nerve fiber layer.
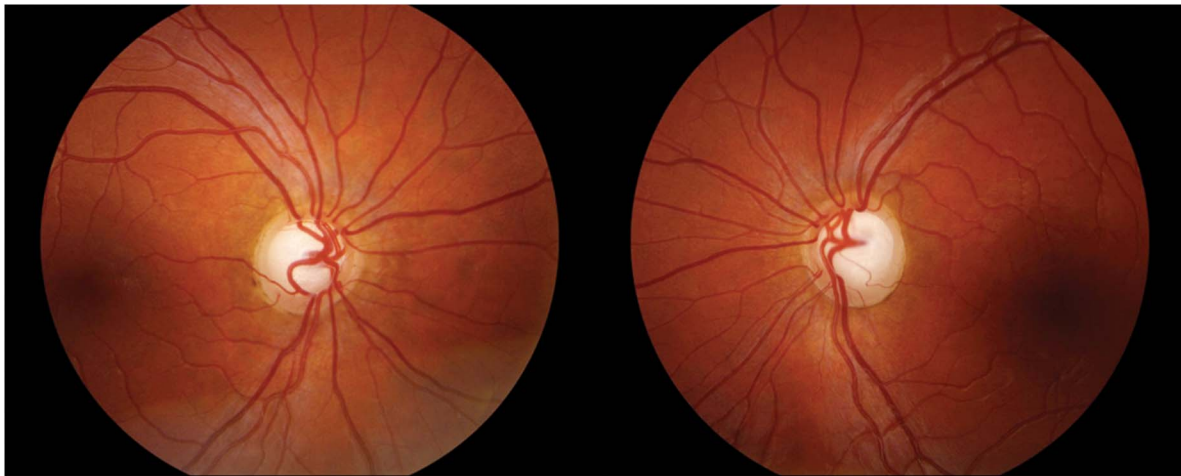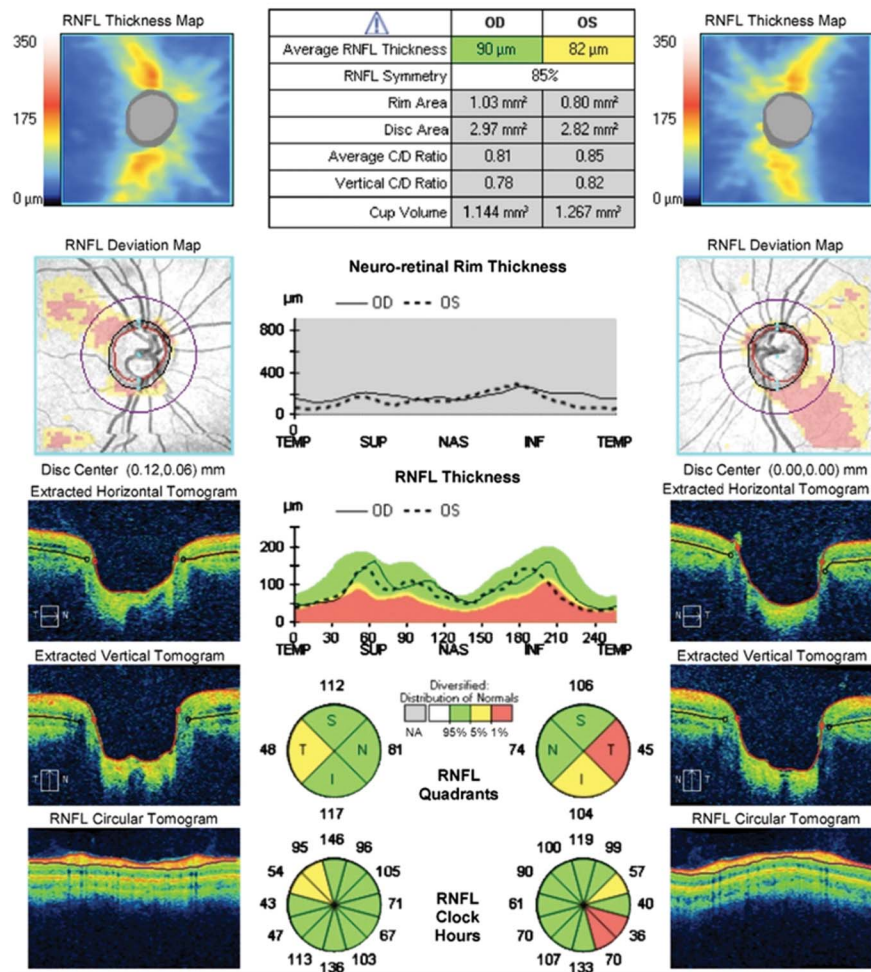
FIG. 12. A large optic nerve can give the appearance of an enlarged cup-to-disc ratio. This patient was referred for evaluation of presumed glaucomatous optic neuropathy. Fundus photography demonstrates large optic nerves with large cup-disc ratios. OCT of the optic nerve demonstrates a large disc area of almost 3 mm² with a relatively normal average RNFL thickness. Note that the abnormal RNFL probability map for the superior arcuate sector in the right eye and the inferior arcuate sector in the left eye are due to the more vertical angle of entry of these arcuate bundles, which is evident on the color thickness map plot and the vertical angle of entrance of the arterial branches corresponding to these bundles. This confirms the diagnosis of megalopapilla, which causes an enlarged cup-to-disc ratio in the absence of true glaucomatous optic neuropathy. OCT, optical coherence tomography; RNFL, retinal nerve fiber layer.

inner layers of the macula, specifically the GCL-IPL complex (60). Unfortunately, the commercially available segmentation algorithms are prone to segmentation failures of the GCL-IPL complex, especially when there is low signal strength, optic nerve edema, or structural abnormalities in the outer retinal layers (which affects segmentation of the inner retinal layers) (61–63). One sign of inaccurate inner layer segmentation is the appearance of nonpathologic
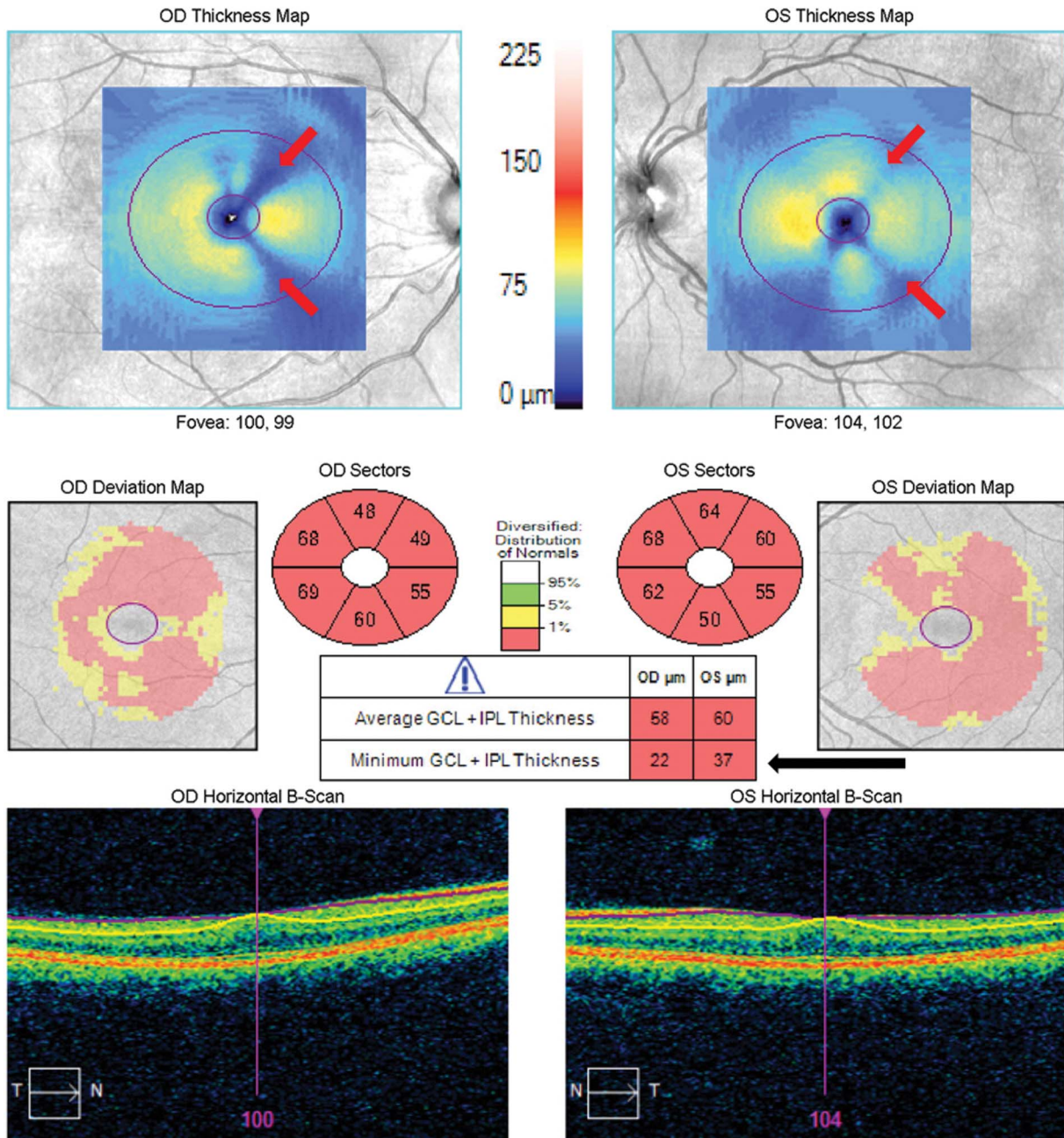
FIG. 13. Errors in segmentation of the GCL-IPL complex. This patient has ocular hypertension with normal automated fields, but the GCL-IPL thickness was artificially decreased due to errors in segmentation. This can be seen as spokes of blue "thinning" in the thickness map or "propeller sign" (*red arrows*). The minimum thickness of the GCL-IPL thickness is less than 40 μm in both eyes (*black arrow*), which is also often an indication of an error in segmentation, especially when the average GCL-IPL thickness value is significantly greater than the minimum thickness (e.g., 68 microns vs 22 microns for the right eye shown here). GCL-IPL, ganglion cell layer-inner plexiform layer.

shapes in the thickness and probability maps, such as a corner of abnormal thinning (Figs. 2, 3). Errors in GCL-IPL segmentation can also often appear as segments of blue (thinning) on the thickness map in the shape of spokes on a wheel ("propeller sign" in Fig. 13). A GCL-IPL reading of less than 40 μm is also typically indicative of areas of segmentation error. On the B-scan, the algorithm's identification of the boundaries of the ganglion cell layer and inner plexiform layer often collapse together in the areas of artifact, producing an artifactual thinning (Figs. 2, 3). More robust 3D segmentation algorithms available in research are able to overcome these segmentation errors (Fig. 2) (12).

Interindividual Variation in Retinal Ganglion Cell Thickness Across the Macula

Within the macula, the most variation in thickness among normal eyes is in the perifoveal location due to a wide variation in thickness profile of the inner retina immediately surrounding the fovea. Therefore, an abnormal probability map in the perifoveal location should be scrutinized carefully and correlated with the clinical exam and functional tests. It is important to ensure that the fovea was correctly identified and centered by the OCT analysis; otherwise, artifactual thickening and thinning of the retina will be displayed as abnormal. However, true atrophy of the GCL-IPL may also cause perifoveal thinning and enlargement of the foveal depression, making it difficult to differentiate focal pathological thinning in the perifoveal inner retina compared to normal variation in thickness in this location.

REPEATABILITY

The repeatability of scans is dependent on a number of factors. It is important to scan the same retinal location with each subsequent examination. Comparing slightly different retinal areas of a scan can lead to an increase in variability, especially in pathologic eyes such as those with macular or optic nerve edema. Many OCT machines have the capability of registration, which will match each subsequent OCT image to a reference baseline scan using landmarks such as the position of retinal vessels and the location of the optic disc. This has been demonstrated to decrease the variability between subsequent scans (2). In addition, newer OCT machines have implemented a gaze tracker, which improves repeatability of subsequent scans. Faster scanning, as will become available with swept source OCT, will also improve reproducibility since retina movements occurring during scans acquired at a faster rate will have less influence.

It is important to note that measurements from different OCT machines cannot be compared directly for a given patient (2,64–68). Different OCT machines provide different thickness measurements because of the differences in the way the scans are obtained, which includes scan speed and number and density of scans obtained. In addition, the

commercially available OCT machines each have their own different, proprietary algorithm that may segment the layers differently. For example, Stratus OCT measures the total macular thickness with boundaries between the internal limiting membrane and the hyper-reflective band corresponding to the interface between the inner and the outer segment of photoreceptors while Spectralis OCT uses the boundaries of the internal limiting membrane and the retinal pigment epithelium to measure the total macular thickness of the retina (64). The differences in the algorithm's defined boundaries of the retina are exaggerated in pathologic eyes, such as choroidal neovascularization from macular degeneration (64).

In addition to using different reference boundaries to define thickness, the specific algorithm used for segmentation can influence repeatability measurements. Sohn et al (69) analyzed the intervisit variability of Spectralis OCT obtained macular thickness measurements from patients with diabetic macular edema and found that an independent 3-dimensional graph segmentation algorithm, the Iowa Reference Algorithm, had slightly better repeatability compared to the manufacturer Spectralis algorithm when analyzing the same Spectralis spectral domain OCT images.

SYSTEMATIC APPROACH TO INTERPRETING OPTIC NERVE AND GANGLION CELL OPTICAL COHERENCE TOMOGRAPHY SCANS

Much like the systematic approach recommended for interpreting automated Humphrey visual fields, we propose a similar approach to interpreting OCT scans.

1. Confirm the name and age of the patient

   • Measurements are made against age matched controls

2. Check signal strength

   • Signal strength ≥7 out of 10 is preferable (for Cirrus OCT)

3. Check refractive error and, if available, axial eye length

   • Axial eye length is particularly helpful for patients who are pseudophakic or who have had refractive surgery

4. Interpretation of the optic disc OCT

   • Examine the thickness and probability retina maps for the presence of rectangular areas of absolute RNFL loss that do not match the anatomical distribution of RNFL arcuate bundles. Nonanatomical areas of loss typically indicate errors in segmentation

- Compare the fundus image and thickness maps to ensure that the identification of the disc border and cup by OCT corresponds to the clinical estimation.
- Compare the OCT-based fundus image or en face image with the superimposed probability map for evidence of ocular torsion and to assess the angle of exit of the branches of the retinal arteries from the disc, which help predict the distribution of the arcuate nerve bundle locations.
- Examine the TSNIT RNFL plot and make note of whether the location of the peaks correspond to the peaks from the normative database. Common associations with discrepancy: long or short axial eye length, abnormal location of vessels as they exit the disc, and ocular torsion. Local areas with a thickness less than 40 μm are typically due to errors in segmentation unless the patient has long-standing severe optic neuropathy.

5. Recognize that ocular disease can create errors in segmentation

- The macular GCL-IPL thickness measurement is especially prone to segmentation error, especially in the presence of optic disc edema and outer photoreceptor disease (e.g., macular degeneration). A GCL-IPL thickness less than 40 μm is typically due to errors in segmentation unless the patient has long-standing severe optic neuropathy.

6. Interpretation of subsequent scans for estimating progression of disease

- Measurements from different brands of OCT machines cannot be directly compared.
- Ensure that the same scan location is compared between sequential scans

CONCLUSIONS

OCT has revolutionized the ability to detect subtle optic nerve disease. However, misinterpretation of artifacts on OCT can lead to errors in clinical judgment, where both false reassurance and false concern can be created. Using a systematic approach to OCT analysis allows one to identify and interpret these artifacts. It is important to note that OCT technology is constantly evolving. Much like spectral domain OCT has largely supplanted time-domain OCT, a new method of faster and more detailed imaging, such as swept source imaging, will likely replace spectral domain OCT in the future. New technology will bring new insight into disease processes, but will likely also bring new artifacts that we will need to be prepared to identify and interpret correctly. Regardless of the future changes in OCT imaging, keeping a systematic approach to OCT analysis

will allow us to avoid or minimize the clinical misinterpretations of artifacts on OCT.

LITERATURE SEARCH

A literature search using PubMed was performed for the keywords *optical coherence tomography, retinal nerve fiber layer thickness, ganglion cell layer-inner plexiform layer, artifact, refractive error*. Each outline subheadings were developed after literature review and was used as an additional keyword. The search was expanded as necessary using the related articles function with PubMed. Only peer-reviewed articles and original descriptions were considered. Articles were excluded if an abstract in English was not available.

REFERENCES

1. **Huang D,** Swanson EA, Lin CP, Schuman JS, Stinson WG, Chang W, Hee MR, Flotte T, Gregory K, Puliafito CA. Optical coherence tomography. Science. 1991;254:1178–1181.
2. **Wolf-Schnurrbusch UE,** Ceklic L, Brinkmann CK, Iliev ME, Frey M, Rothenbuehler SP, Enzmann V, Wolf S. Macular thickness measurements in healthy eyes using six different optical coherence tomography instruments. Invest Ophthalmol Vis Sci. 2009;50:3432–3437.
3. **Sharma A,** Oakley JD, Schiffman JC, Budenz DL, Anderson DR. Comparison of automated analysis of Cirrus HD OCT spectral-domain optical coherence tomography with stereo photographs of the optic disc. Ophthalmology. 2011;118:1348–1357.
4. **Akiyama H,** Kashima T, Li D, Shimoda Y, Mukai R, Kishi S. Retinal ganglion cell analysis in Leber's hereditary optic neuropathy. Ophthalmology. 2013;120:1943–1944.e5.
5. **Medeiros FA,** Lisboa R, Weinreb RN, Liebmann JM, Girkin C, Zangwill LM. Retinal ganglion cell count estimates associated with early development of visual field defects in glaucoma. Ophthalmology. 2013;120:736–744.
6. **Cho JW,** Sung KR, Lee S, Yun SC, Kang SY, Choi J, Na JH, Lee Y, Kook MS. Relationship between visual field sensitivity and macular ganglion cell complex thickness as measured by spectral-domain optical coherence tomography. Invest Ophthalmol Vis Sci. 2010;51:6401–6407.
7. **Tan O,** Chopra V, Lu AT, Schuman JS, Ishikawa H, Wollstein G, Varma R, Huang D. Detection of macular ganglion cell loss in glaucoma by Fourier-domain optical coherence tomography. Ophthalmology. 2009;116:2305–2314.
8. **Gu S,** Glaug N, Cnaan A, Packer RJ, Avery RA. Ganglion cell layer-inner plexiform layer thickness and vision loss in young children with optic pathway gliomas. Invest Ophthalmol Vis Sci. 2014;55:1402–1408.
9. **Mwanza JC,** Durbin MK, Budenz DL, Sayyad FE, Chang RT, Neelakantan A, Godfrey DG, Carter R, Crandall AS. Glaucoma diagnostic accuracy of ganglion cell-inner plexiform layer thickness: comparison with nerve fiber layer and optic nerve head. Ophthalmology. 2012;119:1151–1158.
10. **Walter SD,** Ishikawa H, Galetta KM, Sakai RE, Feller DJ, Henderson SB, Wilson JA, Maguire MG, Galetta SL, Frohman E, Calabresi PA, Schuman JS, Balcer LJ. Ganglion cell loss in relation to visual disability in multiple sclerosis. Ophthalmology. 2012;119:1250–1257.
11. **Ronnback C,** Milea D, Larsen M. Imaging of the macula indicates early completion of structural deficit in autosomal-dominant optic atrophy. Ophthalmology. 2013;120:2672–2677.
12. **Chen JJ,** Thurtell MJ, Longmuir RA, Garvin MK, Wang JK, Wall M, Kardon RH. Causes and prognosis of visual acuity loss at the time of initial presentation in idiopathic intracranial hypertension. Invest Ophthalmol Vis Sci. 2015;56:3850–3859.

13. **Kim NR,** Lim H, Kim JH, Rho SS, Seong GJ, Kim CY. Factors associated with false positives in retinal nerve fiber layer color codes from spectral-domain optical coherence tomography. Ophthalmology. 2011;118:1774–1781.
14. **Asrani S,** Essaid L, Alder BD, Santiago-Turla C. Artifacts in spectral-domain optical coherence tomography measurements in glaucoma. JAMA Ophthalmol. 2014.
15. **Kim KE,** Jeoung JW, Park KH, Kim DM, Kim SH. Diagnostic classification of macular ganglion cell and retinal nerve fiber layer analysis: differentiation of false-positives from glaucoma. Ophthalmology. 2015;122:502–510.
16. **Budenz DL,** Anderson DR, Varma R, Schuman J, Cantor L, Savell J, Greenfield DS, Patella VM, Quigley HA, Tielsch J. Determinants of normal retinal nerve fiber layer thickness measured by Stratus OCT. Ophthalmology. 2007;114:1046–1052.
17. **Parikh RS,** Parikh SR, Sekhar GC, Prabakaran S, Babu JG, Thomas R. Normal age-related decay of retinal nerve fiber layer thickness. Ophthalmology. 2007;114:921–926.
18. **Celebi AR,** Mirza GE. Age-related change in retinal nerve fiber layer thickness measured with spectral domain optical coherence tomography. Invest Ophthalmol Vis Sci. 2013;54:8095–8103.
19. **Leung CK,** Ye C, Weinreb RN, Yu M, Lai G, Lam DS. Impact of age-related change of retinal nerve fiber layer and macular thicknesses on evaluation of glaucoma progression. Ophthalmology. 2013;120:2485–2492.
20. **Cheung CY,** Leung CK, Lin D, Pang CP, Lam DS. Relationship between retinal nerve fiber layer measurement and signal strength in optical coherence tomography. Ophthalmology. 2008;115:1347–1351.
21. **Wu Z,** Huang J, Dustin L, Sadda SR. Signal strength is an important determinant of accuracy of nerve fiber layer thickness measurement by optical coherence tomography. J Glaucoma. 2009;18:213–216.
22. **Vizzeri G,** Bowd C, Medeiros FA, Weinreb RN, Zangwill LM. Effect of signal strength and improper alignment on the variability of stratus optical coherence tomography retinal nerve fiber layer thickness measurements. Am J Ophthalmol. 2009;148:249–255.
23. **Vizzeri G,** Bowd C, Medeiros FA, Weinreb RN, Zangwill LM. Effect of improper scan alignment on retinal nerve fiber layer thickness measurements using Stratus optical coherence tomograph. J Glaucoma. 2008;17:341–349.
24. **Chan CK,** Miller NR. Peripapillary nerve fiber layer thickness measured by optical coherence tomography in patients with no light perception from long-standing nonglaucomatous optic neuropathies. J Neuroophthalmol. 2007;27:176–179.
25. **Groth SL,** Harrison A, Grajewski AL, Lee MS. Retinal nerve fiber layer thickness using spectral-domain optical coherence tomography in patients with no light perception secondary to optic atrophy. J Neuroophthalmol. 2013;33:37–39.
26. **Mitchell P,** Hourihan F, Sandbach J, Wang JJ. The relationship between glaucoma and myopia: the Blue Mountains Eye Study. Ophthalmology. 1999;106:2010–2015.
27. **Shoji T,** Nagaoka Y, Sato H, Chihara E. Impact of high myopia on the performance of SD-OCT parameters to detect glaucoma. Graefe's Arch Clin Exp Ophthalmol. 2012;250:1843–1849.
28. **Kang SH,** Hong SW, Im SK, Lee SH, Ahn MD. Effect of myopia on the thickness of the retinal nerve fiber layer measured by Cirrus HD optical coherence tomography. Invest Ophthalmol Vis Sci. 2010;51:4075–4083.
29. **Leung CK,** Mohamed S, Leung KS, Cheung CY, Chan SL, Cheng DK, Lee AK, Leung GY, Rao SK, Lam DS. Retinal nerve fiber layer measurements in myopia: an optical coherence tomography study. Invest Ophthalmol Vis Sci. 2006;47:5171–5176.
30. **Rauscher FM,** Sekhon N, Feuer WJ, Budenz DL. Myopia affects retinal nerve fiber layer measurements as determined by optical coherence tomography. J Glaucoma. 2009;18:501–505.
31. **Savini G,** Barboni P, Parisi V, Carbonelli M. The influence of axial length on retinal nerve fibre layer thickness and optic-disc size measurements by spectral-domain OCT. Br J Ophthalmol. 2012;96:57–661.
32. **Choi SW,** Lee SJ. Thickness changes in the fovea and peripapillary retinal nerve fiber layer depend on the degree of myopia. Korean J Ophthalmol. 2006;20:215–219.
33. **Hougaard JL,** Ostenfeld C, Heijl A, Bengtsson B. Modelling the normal retinal nerve fibre layer thickness as measured by Stratus optical coherence tomography. Graefe's Arch Clin Exp Ophthalmol. 2006;244:1607–1614.
34. **Kim MJ,** Lee EJ, Kim TW. Peripapillary retinal nerve fibre layer thickness profile in subjects with myopia measured using the Stratus optical coherence tomography. Br J Ophthalmol. 2010;94:115–120.
35. **Wang G,** Qiu KL, Lu XH, Sun LX, Liao XJ, Chen HL, Zhang MZ. The effect of myopia on retinal nerve fibre layer measurement: a comparative study of spectral-domain optical coherence tomography and scanning laser polarimetry. Br J Ophthalmol. 2011;95:255–260.
36. **Leung CK,** Cheng AC, Chong KK, Leung KS, Mohamed S, Lau CS, Cheung CY, Chu GC, Lai RY, Pang CC, Lam DS. Optic disc measurements in myopia with optical coherence tomography and confocal scanning laser ophthalmoscopy. Invest Ophthalmol Vis Sci. 2007;48:3178–3183.
37. **Jonas JB,** Budde WM, Panda-Jonas S. Ophthalmoscopic evaluation of the optic nerve head. Surv Ophthalmol. 1999;43:293–320.
38. **Jonas JB**. Optic disk size correlated with refractive error. Am J Ophthalmol. 2005;139:346–348.
39. **Dementyev DD,** Kourenkov VV, Rodin AS, Fadeykina TL, Diaz Martines TE. Retinal nerve fiber layer changes after LASIK evaluated with optical coherence tomography. J Refrat Surg. 2005;21:S623–S627.
40. **Sharma N,** Sony P, Gupta A, Vajpayee RB. Effect of laser in situ keratomileusis and laser-assisted subepithelial keratectomy on retinal nerve fiber layer thickness. J Cataract Refract Surg. 2006;32:446–450.
41. **Bennett AG,** Rudnicka AR, Edgar DF. Improvements on Littmann's method of determining the size of retinal features by fundus photography. Graefe's Arch Clin Exp Ophthalmol. 1994;232:361–367.
42. **Hong SW,** Ahn MD, Kang SH, Im SK. Analysis of peripapillary retinal nerve fiber distribution in normal young adults. Invest Ophthalmol Vis Sci. 2010;51:3515–3523.
43. **Hwang YH,** Yoo C, Kim YY. Characteristics of peripapillary retinal nerve fiber layer thickness in eyes with myopic optic disc tilt and rotation. J Glaucoma. 2012;21:394–400.
44. **Hwang YH,** Yoo C, Kim YY. Myopic optic disc tilt and the characteristics of peripapillary retinal nerve fiber layer thickness measured by spectral-domain optical coherence tomography. J Glaucoma. 2012;21:260–265.
45. **Yoo YC,** Lee CM, Park JH. Changes in peripapillary retinal nerve fiber layer distribution by axial length. Optom Vis Sci. 2012;89:4–11.
46. **Yamashita T,** Asaoka R, Tanaka M, Kii Y, Yamashita T, Nakao K, Sakamoto T. Relationship between position of peak retinal nerve fiber layer thickness and retinal arteries on sectoral retinal nerve fiber layer thickness. Invest Ophthalmol Vis Sci. 2013;54:5481–5488.
47. **Yamashita T,** Kii Y, Tanaka M, Yoshinaga W, Yamashita T, Nakao K, Sakamoto T. Relationship between supernormal sectors of retinal nerve fibre layer and axial length in normal eyes. Acta Ophthalmol. 2014.
48. **Hong S,** Kim CY, Seong GJ. Adjusted peripapillary retinal nerve fiber layer thickness measurements based on the optic nerve head scan angle. Invest Ophthalmol Vis Sci. 2010;51:4067–4074.
49. **Hood DC,** Fortune B, Arthur SN, Xing D, Salant JA, Ritch R, Liebmann JM. Blood vessel contributions to retinal nerve fiber layer thickness profiles measured with optical coherence tomography. J Glaucoma. 2008;17:519–528.
50. **Carmeliet P,** Tessier-Lavigne M. Common mechanisms of nerve and blood vessel wiring. Nature. 2005;436:193–200.
51. **Miller G**. Developmental biology. Nerves tell arteries to make like a tree. Science. 2002;296:2121–2123.

52. **Lee KH,** Kim CY, Kim NR. Variations of retinal nerve fiber layer thickness and ganglion cell-inner plexiform layer thickness according to the torsion direction of optic disc. Invest Ophthalmol Vis Sci. 2014;55:1048–1055.

53. **Hwang YH,** Lee JY, Kim YY. The effect of head tilt on the measurements of retinal nerve fibre layer and macular thickness by spectral-domain optical coherence tomography. Br J Ophthalmol. 2011;95:1547–1551.

54. **Valverde-Megias A,** Martinez-de-la-Casa JM, Serrador-Garcia M, Larrosa JM, Garcia-Feijoo J. Clinical relevance of foveal location on retinal nerve fiber layer thickness using the new FoDi software in Spectralis optical coherence tomography. Invest Ophthalmol Vis Sci. 2013;54:5771–5776.

55. **Hood DC,** Raza AS, de Moraes CG, Liebmann JM, Ritch R. Glaucomatous damage of the macula. Prog Retin Eye Res. 2013;32:1–21.

56. **Chen JJ,** Kardon RH, Longmuir RA. Diagnostic features of retinal nerve fiber layer rotation in skew deviation using optical coherence tomography. J Neuroophthalmol. 2014;34:389–392.

57. **Kim SY,** Park HY, Park CK. The effects of peripapillary atrophy on the diagnostic ability of Stratus and Cirrus OCT in the analysis of optic nerve head parameters and disc size. Invest Ophthalmol Vis Sci. 2012;53:4475–4484.

58. **Jonas JB,** Nguyen XN, Gusek GC, Naumann GO. Parapapillary chorioretinal atrophy in normal and glaucoma eyes. I. Morphometric data. Invest Ophthalmol Vis Sci. 1989;30:908–918.

59. **Thurtell MJ,** Tomsak RL, Daroff RB. Neuro-Ophthalmology. New York: Oxford University Press, 2012.

60. **Kardon RH**. Role of the macular optical coherence tomography scan in neuro-ophthalmology. J Neuroophthalmol. 2011;31:353–361.

61. **Lee K,** Niemeijer M, Garvin MK, Kwon YH, Sonka M, Abramoff MD. Segmentation of the optic disc in 3-D OCT scans of the optic nerve head. IEEE Trans Med Imaging. 2010;29:159–168.

62. **Garvin MK,** Abramoff MD, Kardon R, Russell SR, Wu X, Sonka M. Intraretinal layer segmentation of macular optical coherence tomography images using optimal 3-D graph search. IEEE Trans Med Imaging. 2008;27:1495–1505.

63. **Garvin MK,** Abramoff MD, Wu X, Russell SR, Burns TL, Sonka M. Automated 3-D intraretinal layer segmentation of macular spectral-domain optical coherence tomography images. IEEE Trans Med Imaging. 2009;28:1436–1447.

64. **Giani A,** Cigada M, Choudhry N, Deiro AP, Oldani M, Pellegrini M, Inverneizzi A, Duca P, Miller JW, Staurenghi G. Reproducibility of retinal thickness measurements on normal and pathologic eyes by different optical coherence tomography instruments. Am J Ophthalmol. 2010;150:815–824.

65. **Sung KR,** Kim DY, Park SB, Kook MS. Comparison of retinal nerve fiber layer thickness measured by Cirrus HD and Stratus optical coherence tomography. Ophthalmology. 2009;116:1264–1270.

66. **Leite MT,** Rao HL, Weinreb RN, Zangwill LM, Bowd C, Sample PA, Talfreshi A, Medeiros FA. Agreement among spectral-domain optical coherence tomography instruments for assessing retinal nerve fiber layer thickness. Am J Ophthalmol. 2011;151:85–92.

67. **Seibold LK,** Mandava N, Kahook MY. Comparison of retinal nerve fiber layer thickness in normal eyes using time-domain and spectral-domain optical coherence tomography. Am J Ophthalmol. 2010;150:807–814.

68. **Pierro L,** Giatsidis SM, Mantovani E, Gagliardi M. Macular thickness interoperator and intraoperator reproducibility in healthy eyes using 7 optical coherence tomography instruments. Am J Ophthalmol. 2010;150:199–204.

69. **Sohn EH,** Chen JJ, Lee K, Niemeijer M, Sonka M, Abramoff MD. Reproducibility of diabetic macular edema estimates from SD-OCT is affected by the choice of image analysis algorithm. Invest Ophthalmol Vis Sci. 2013;54:4184–4188.